

A Study of the Ice-Hail Charge Separation Mechanism
Using a Thunderstorm Electrification Model with
Explicit Microphysics in a Kinematic Framework.

by

Kent W. Norville

A dissertation submitted in partial fulfillment
of the requirements for the degree of

Doctor of Philosophy

University of Washington

1990

Approved by Mervin Baker

(Chairperson of Supervisory Committee)

[Signature]

R. A. Houze

L. B. Sorensen

Program Authorized
to Offer Degree _____

Date _____

A Study of the Ice-Hail Charge Separation Mechanism
Using a Thunderstorm Electrification Model with
Explicit Microphysics in a Kinematic Framework.

by

Kent W. Norville

A dissertation submitted in partial fulfillment
of the requirements for the degree of

Doctor of Philosophy

University of Washington

1990

Approved by Mervin Baker

(Chairperson of Supervisory Committee)

[Signature]

R. A. Houze

L. B. Sorensen

Program Authorized
to Offer Degree _____

Date _____

Doctoral Dissertation

In presenting this dissertation in partial fulfillment of the requirements for the Doctoral degree at the University of Washington, I agree that the Library shall make its copies freely available for inspection. I further agree that extensive copying of this dissertation is allowable only for scholarly purposes, consistent with "fair use" as prescribed in the U.S. Copyright Law. Requests for copying or reproduction of this dissertation may be referred to University Microfilms, 300 North Zeeb Road, Ann Arbor, Michigan 48106, to whom the author has granted "the right to reproduce and sell (a) copies of the manuscript in microform and/or (b) printed copies of the manuscript made from microform."

Signature _____

Date _____

University of Washington

Abstract

A Study of the Ice-Hail Charge Separation Mechanism
Using a Thunderstorm Electrification Model with
Explicit Microphysics in a Kinematic Framework.

by Kent W. Norville

Chairperson of the Supervisory Committee: Professor Marcia B. Baker
Geophysics Program

I have developed a numerical model for examining the thunderstorm electrification process assuming that the electrification is entirely due to non-inductive charge transfer between colliding ice crystals and hail. Since this ice-hail charge mechanism is very dependent on particle sizes and distributions, 78 categories of ice and 30 categories of drops are used in an explicit microphysical framework. To maintain simplicity, the electrification model has a kinematic structure; thus the temperature and velocity fields are input into the electrification model. These fields can be either calculated by a background model or retrieved from observation. For this study, we have used the cloud model of Taylor (1989) to generate the temperature and velocity fields to examine the July 19, 1981 CCOPE thundercloud. Using these fields, the electrification model produced time-dependent ice particle concentrations, radar reflectivities, charge and vertical electric field distributions in good general agreement with those observed. The model produced a maximum electric field strength of 2.34 kV-cm^{-1} , which on the same order of that needed for lightning initiation, and occurred very close to the time of the observed discharge. Thus the ice-hail charge mechanism by itself seems capable of explaining the electrical development in storms such as the July 19th cloud. The details of the electrification depended on the liquid water content and the glaciation processes. Specifically, I found that the locations of the charge centers were directly related to the interface between mixed-phase and completely glaciated cloud. The electrification was strongly dependent on the ice crystal characteristics. Specifically, cases where the crystals grew to riming sizes ($> 400\mu$)

fastest charge most efficiently. However, the characteristics of the large riming ice only had a minor influence on the charging. The electrification was not sensitive to charge transfer critical diameter or the initial drop distribution. The electrification was sensitive to ice-ice sticking efficiency as predicted.

TABLE OF CONTENTS

List of Figures	v
List of Tables	vii
Chapter 1 Introduction	1
1.1 Electrical characteristics of a thunderstorm	1
1.2 Observational constraints on the charge separation mechanism	2
1.3 Summary of charge separation mechanisms	3
1.4 Description of the ice-hail non-inductive charge separation mechanism	4
1.5 Previous model studies of non-inductive charging.	6
1.6 Goals of this work	9
1.7 Organization of this dissertation	9
Chapter 2 Electrical/Microphysical (EM) Model Development	10
2.1 Model geometry and advection scheme	12
2.2 Particle characteristics	15
2.2.1 Mass grid	15
2.2.2 Ice density parameterization	15
2.2.3 Fall velocities	16
2.3 Microphysical equations	16
2.3.1 Deposition	16
2.3.2 Particle redistribution	18
2.3.3 Particle interactions: collisions and collection	18
2.3.4 Ice formation	20
2.4 Electrification equations	21
2.5 Model limitations and omissions	24
Chapter 3 Base Case Description and EM Initialization	26

3.1	Description of CCOPE July 19 case study	26
3.2	Background model	26
3.3	EM initialization	29
3.4	Base case description	30
Chapter 4 Base Case Analysis		32
4.1	Microphysical analysis	32
4.1.1	Reflectivity factor(dBZ_e)	32
4.1.2	Thermodynamic analysis	38
4.1.3	Particle distributions	41
4.1.4	Microphysical summary	43
4.2	Electrical analysis	43
4.2.1	Charge density	43
4.2.2	Particle charge distributions	48
4.2.3	Electric field on the axis, E_a	51
4.3	Summary	56
Chapter 5 Sensitivity Tests		58
5.1	Ice density parameterization	58
5.1.1	Ice crystal density - ρ_{crys}	58
5.1.2	Initial riming diameter - D_r	60
5.1.3	Accretion riming type - ρ_a	64
5.2	Ice nucleation concentration	67
5.3	Mixing	71
5.4	Stick efficiency - E_{si}	76
5.5	Drop distribution	77
5.6	Critical charge transfer diameter - D_{crit}	78
5.7	Summary	80
Chapter 6 Discussion		81

6.1	Assessment of the role of the ice-hail non-inductive charge separation mechanism in thunderstorm electrification.	81
6.2	Thunderstorm electrification.	83
Chapter 7	Conclusions and Final Remarks	84
7.1	Summary of this work	84
7.2	Suggestions for future work	85
	References	87
Appendix A	Derivation of Advective Equations.	94
Appendix B	Crystal density determination.	96
Appendix C	Derivation of Z to Z_e ice correction	98

LIST OF FIGURES

1.1	Cartoon of the non-inductive ice-hail charge separation mechanism . . .	5
2.1	EM model schematic with inputs and outputs.	11
2.2	The model geometry	13
2.3	Charge transferred per collision vs. small crystal diameter	23
3.1	Inner and outer region vertical velocity profiles as input to the EM model	28
4.1	Time-height profiles for calculated T and EM model inner region re- flectivities.	34
4.2	Inner region liquid water mixing ratios for the T and EM model with King Air observations.	35
4.3	Time-height profiles for observed and EM model reflectivities.	37
4.4	Time-height profiles for calculated EM inner and outer region reflectivity.	39
4.5	Paluch diagram at 481 mb: T and EM Models and Observations	40
4.6	EM model ice spectra at 3400 seconds.	42
4.7	Time-height profiles for EM ice and graupel concentrations	44
4.8	Inner region calculated time-height contours of positive, negative, and net charge density and liquid water mixing ratio.	45
4.9	Total positive, negative and net charge accumulated in the inner region	47
4.10	Charge per particle for the base case run	49
4.11	Charge concentrations of each mass category and height level.	52
4.12	Calculated time-height profile of the electric field on the axis	53
4.13	Electric field values at 5.8 km as a function of time: Model and ob- servations	55
5.1	Ice particle density profiles used in the ice crystal sensitivity runs	59

5.2	Time-height reflectivity profiles for the ρ_{crys} runs	61
5.3	Ice particle density profiles used in the D_r sensitivity runs	63
5.4	Particle density vs. diameter for the various accretion density formulas.	65
5.5	Ice particle spectra for different riming parameterizations	66
5.6	Ice nucleation concentrations vs. temperature of the four ice nucleations runs	69
5.7	Total negative charge in the inner region for ice nucleation type runs	70
5.8	Time-height profiles for the inner region net charge density for ice nucleation type runs	72
5.9	Time-height profile of the net charge density for the enhanced mixing run.	73
5.10	Mean charge per particle distributions for the base and mixed runs. .	75
5.11	Magnitude of the charge per particle and total charge density per particle curves for the D_{crit} runs	79

LIST OF TABLES

1.1 Non-Inductive Model Characteristics 7

3.1 Comparison of Models with Observation 29

3.2 Base Run Parameter Settings 31

4.1 Base run and observation summary 56

5.1 Ice crystal density ρ_{crys} summary 60

5.2 D_r summary 62

5.3 Accretion density run descriptions 67

5.4 Ice nucleation run summary 68

5.5 Mixing summary 74

5.6 Stick efficiency run summary 76

5.7 Drop distribution electrification summary 77

5.8 D_{crit} summary 78

B.1 Calculated densities assuming sphere with same radius as an equal
mass plate 97

Acknowledgements

Before and during my graduate career at the University of Washington, many people have help me along the road toward my Doctorate. Although many of them have not "directly" contributed in my research, all, in one way or another, have contributed to my personal growth for which I am grateful. I am thankful for the friends I have met here in Seattle and for those outside of Seattle who have kept contact over the years. I wish to express thanks to everyone in the the Space Sciences and Cloud groups for good discussions, company, assistance, and support.

Several persons deserve special acknowledgement. I would like to express my upmost gratitude to my thesis advisor, Marcia Baker, who provide me with insight, guidance, support, and hope during my dissertation process. She was there to celebrate the "little" successes with me and to help me through the disappointments. She has taught me much. I am grateful for the careful reading of my dissertation by Professors Marcia Baker, Robert Holzworth, Robert Houze, and John Latham. I would also like to thank Greg Taylor for providing me with his model and code and for many helpful discussions regarding its use. Also, I wold like to thank Professor John Latham for the early discussions and his continued support of this project. I am grateful to Professor Robert Holzworth who initiated my interest in Atmospheric Electricity and has provided me with constant support and encouragement during my graduate career.

And finally, a special thanks to my daughter Racheal for not complaining too loudly when I wanted to look over some work rather than play Barbies.

This research was supported by NASA grant 1738-SS-148.

Chapter 1

Introduction

A lightning storm is one of Nature's most spectacular phenomena. However, the basic physical processes by which a storm electrifies and produces lightning are not understood. In fact, the mechanism(s) responsible for the separation of charge in thunderstorms still remains in dispute. Recent laboratory experiments (Jayaratne et al., 1983; Baker et al., 1987; Keith and Saunders, 1989) have indicated that a non-inductive charge separation mechanism involving ice-hail collisions could be an important candidate for explaining the thunderstorm electrification process. This dissertation describes the development and use of a numerical thunderstorm electrification model to examine the implications of this charge separation mechanism and to understand the electrification process further.

1.1 Electrical characteristics of a thunderstorm

A thunderstorm is generally dipolar in structure, usually with the main positive charge center above the main negative charge center. Sometimes a region of positive charge forms near cloud base but it has a much smaller magnitude than the main centers (Williams, 1989). The negative charge center in a typical summertime thunderstorm is in the temperature range of -10°C to -28°C independent of the cloud base and top temperatures and heights. This observation implies an inherent temperature dependence in the charging process.

Strong electrification is associated with the ice phase. Although there have been reports of lightning in warm clouds (Moore et al., 1960), strong warm cloud electrification is uncommon and requires very special conditions (Williams, 1989). At temperate latitudes, electrification only occurs if the clouds grow past the freezing level (Krehbiel, 1986). For example, Dye et al. (1989) observed that New Mexico storms electrified when the radar tops exceeded 8 km ($T < -20^{\circ}\text{C}$) and lightning was initiated when radar tops rose above 9.5 km ($T \leq -40^{\circ}\text{C}$). They also found that the

initial electrification was associated with vertical motion in the cloud.

Observations also suggest that electrification is dependent on precipitation. The initiation of lightning, which requires breakdown field strengths of about 3 kV-cm^{-1} (Latham, 1981), generally occurs within 20 minutes after the first precipitation detected (Krehbiel, 1986). Typically, lightning is observed when the radar reflectivity above the freezing level exceeds 40 dBZ (Dye et al., 1986) but it has been reported at lower (33-35 dBZ) reflectivities (Moore, 1965). Also, the location of the lightning centers is often observed on the upper fringes of the reflectivity core (Krehbiel, 1986; Lhermitte and Williams, 1985) and not in the highest reflectivity regions.

These observations indicate that initial electrification depends on the ice phase, precipitation, and is inherently temperature dependent.

1.2 Observational constraints on the charge separation mechanism

There is an ongoing debate about which charging processes are primarily responsible for generating the large electric field needed for lightning initiation. Many mechanisms and theories have been proposed (see reviews by Latham (1981), Illingworth (1985), and Beard and Ochs (1986)). There are two main classes of theoretical mechanisms: convective and precipitative. In the convective mechanisms, charge separation takes place outside the cloud (i.e. ionization of the ambient atmosphere by cosmic rays, radiation, and/or corona). Organized cloud motions then move this pre-existing charge to the locations required for electrification (Vonnegut, 1953). In the precipitative mechanisms, the separation of charge occurs in the cloud via hydrometeor interactions. The charges carried by these particles are moved by air motions and/or gravitational settling into the observed distribution. Thus the primary difference between these mechanisms is the location of the original charge separation (external or internal to the cloud).

The thunderstorm observations described above imply that the convective mechanisms of electrification, which cannot account for the observed dependence of electrification on ice and the temperature dependence of the charge centers, are not primarily responsible for thunderstorm electrification (Williams, 1989).

1.3 Summary of charge separation mechanisms

Based on the above observations, it would seem that either ice-ice or ice-water particle interactions might be likely candidates for the primary charge separation mechanism.

Mechanisms depending on water-ice interactions, such as melting (Martin and Hutchinson, 1977), or splashing (Shewchuk and Iribarne, 1971), and/or rebounding of drops (Mason, 1988), cannot explain the electrical development of storms since they require conditions that are not applicable to a wide range of electrified storms (Illingworth, 1985). Also, laboratory experiments do not support these mechanisms. For example, Jennings (1975) found that virtually all drops striking a hail particle were collected when an electric field was present. If a drop did rebound, no detectable charge was observed on it.

This leaves only the ice-ice charge separation mechanisms. There are two main types of ice-ice interactions: inductive and non-inductive.

The inductive mechanism is based on the principle that a particle in an electric field will have polarization charge on its surface. Thus, small rebounding particles will carry charge away when they strike the surface as long as collisions occur below the "electrical equator"¹ of the particle (Sartor, 1981). The inductive mechanism is attractive because it is conceptually simple and provides positive feedback field growth via gravitational separation of charged particles. However, there are several major weaknesses in this mechanism. Illingworth and Caranti (1985) found that the contact time in ice-ice collisions was too short for effective transfer of polarization charge. In fact, they found the inductive mechanism was only effective if the impurity concentration was many orders above the natural impurity levels. There is also a limit on the amount of charge that can be collected via this mechanism and particles have been observed to have charges larger than these limits (Latham, 1981).

In some modeling studies, the inductive processes, when operating alone, produced complex charge distributions and field growth unlike that observed (Kuetner et al., 1981; Tzur and Levin, 1981). Helsdon and Farley (1987a) found, when modelling the CCOPE July 19, 1981 cloud, that the electric field produced using the inductive mechanism alone was about two orders of magnitude too low. In fact, most studies which have compared the inductive and non-inductive mechanisms have

¹The electrical equator can be described as a contour of zero charge density. For an uncharged spherical particle, the electrical equator would be the physical equator normal to the electric field.

found that the inductive charge mechanism by itself cannot adequately explain the electrification.

While inductive charge separation processes require the pre-existence of an electric field, non-inductive processes do not. Three non-inductive mechanisms of the separation of charge during collisions of ice articles have been proposed theoretically: thermoelectric effect (Reynolds et al., 1957), freezing potentials (Workman and Reynolds, 1948), and contact potentials (Caranti et al., 1985). These mechanisms have been shown to be ineffective in laboratory experiments and have been eliminated from consideration in thunderstorm conditions (Latham, 1981). In the next sections I describe laboratory observations of a type of non-inductive charge transfer for which the underlying mechanism is yet unknown but which appears to be operative in clouds.

1.4 Description of the ice-hail non-inductive charge separation mechanism

The non-inductive charge separation mechanism used in this study is based on laboratory observations that collisions between large and small ice particles, while in the presence of liquid water, result in a net charge transfer between the ice particles (see Figure 1.1). In laboratory experiments designed to simulate cloud conditions, Jayaratne et al. (1983) measured the charge transferred to a rotating rod simulating a hailstone in the presence of ice crystals and liquid water. They found the magnitude of the charge per event was a function of ice crystal size (d) and rimer velocity (v). The sign of charge transferred to the rod was generally a function of rime temperature and liquid water content, with positive charge transferred to the rimer at warmer temperatures and higher liquid water content. However, if the liquid water content dropped to zero, the charging was reduced by three orders of magnitude. Also, when ice was absent or when the rimer was stationary, no charging occurred, indicating the importance of both large and small ice crystals. Increasing the liquid water content increased the magnitude of charging and pushed the reversal temperature² (T_r) to lower temperatures. The maximum diameter of ice crystal particles in the experiment was 125μ , but extrapolation of the laboratory results to larger particle sizes suggested that this process could be important in thunderstorm electrification

²the temperature at which the sign of the charge transferred to the rimer changed.

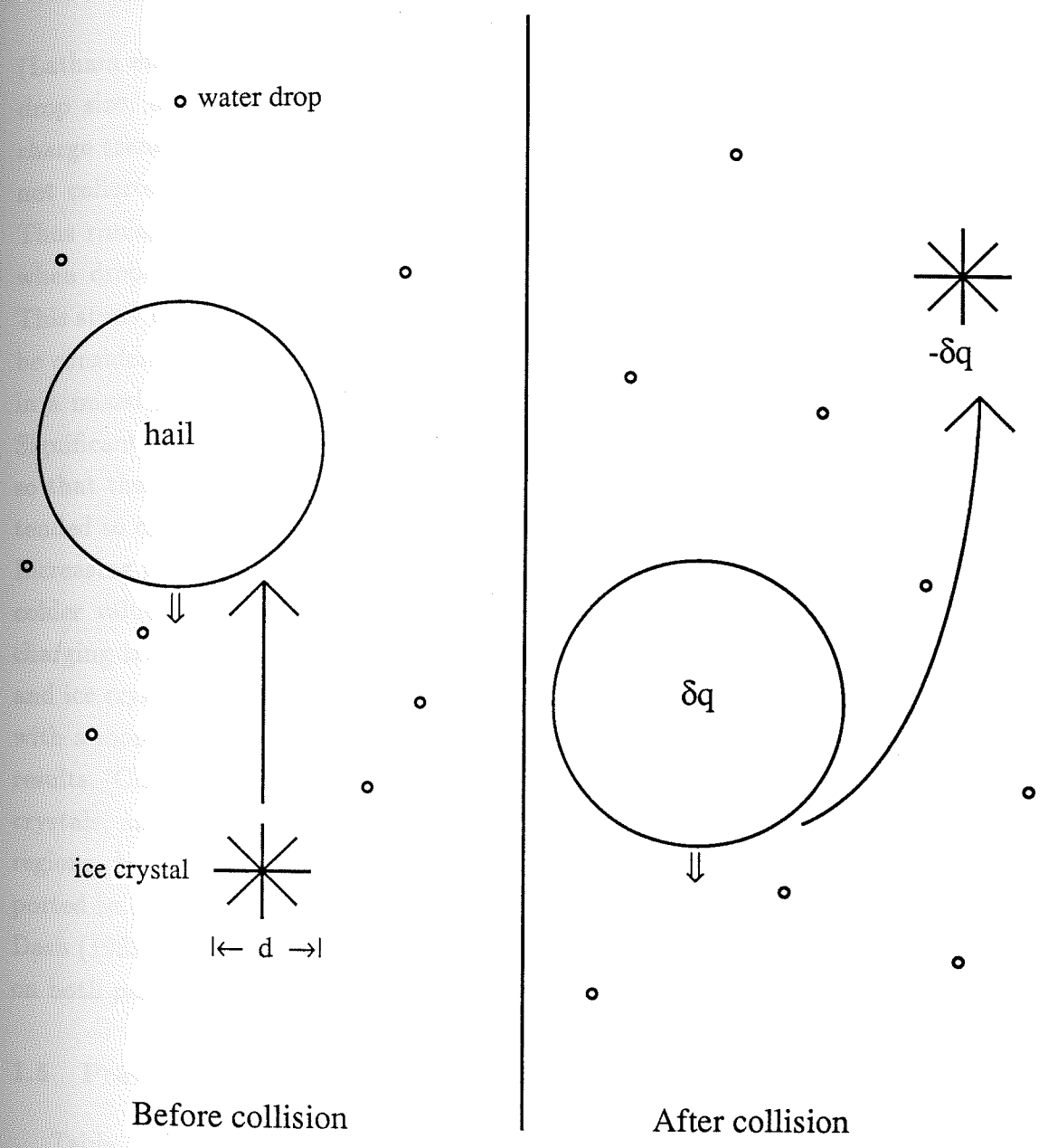


Figure 1.1: Cartoon of the non-inductive ice-hail charge separation mechanism. δq is the charge separated during the ice-hail collision.

(Latham and Dye, 1989). In another study, Jayaratne and Saunders (1985) showed drop size, as well as liquid water content, was important in determining sign of charge transfer. When the drops were less than six microns in diameter, they were not collected by the rimer and the rimer charged negatively at all temperatures. Thus riming was not a necessary condition for charge transfer to occur. However, when drops were collected, the rimer charged positively at warmer temperatures. This study suggested the surface states of both target and interacting particle must be considered. Baker et al. (1987) summarized these results: 1) Charging occurred in a mixed phase cloud during collisions between ice crystals and the hailstone, 2) Significant charging (> 0.1 fC per collision) required the presence of liquid water, so that the hailstone and ice crystal were growing by vapor diffusion, 3) Hailstones tended to charge positively at warmer and negatively at colder temperatures, and 4) Increasing the liquid water content tended to shift the reversal temperature towards colder values and increased charging. Baker et al. suggested that the sign of the charging is dependent on the difference in the depositional growth rates of the hail and ice crystal with the faster growing particle charging positively during a collision with a more slowly growing particle. This description seems to fit the experimental results. Charging would be most likely to occur in regions where liquid water, ice crystals, and hail co-exist. These areas would not be in the strongest precipitation regions, but on the fringes, where liquid water from the updraft could be transported in. The physical basis of this charging mechanism is unknown: Baker and Dash (1989) suggest that the charge transfer is a result of liquid-like layers that form on both particles during deposition.

1.5 Previous model studies of non-inductive charging.

Table 1.1 shows a summary of earlier cold cloud electrification modelling studies that used some form of non-inductive charge transfer. For comparison, the modelling study in this thesis is also included. This table gives a description and the general forms of the charge separation mechanisms for each model. The description indicates the type and geometry of the model, whether the model results were compared with observation, and the type of the microphysics used. Several features of this table are worth noting. First, many of these modelling studies have been used to evaluate different charge mechanisms. As suggested by observations, modellers have generally

Table 1.1:
Non-Inductive Model Characteristics

	Model Description	Charge Mechanisms					
		Inductive			Non-Inductive		
		w-w	w-i	i-i	w-w	w-i	i-i
Illingworth and Latham 1977	1D, SS, slab, BM	X	X	X	X	X	X
Kuettner, Levin, and Sartor 1981	2D, SS, slab, kin, BM		X	X		X	X
Tzur and Levin 1981	1D, TD, axi, EM	X	X	X		X	X
Rawlins 1982	3D, TD, O, BM			X			X
Takahashi 1983	2D, TD, slab, EM			X			X
Takahashi 1984	2D, TD, slab, EM						X
Ziegler, Ray, and MacGorman 1986	3D, TD, kin, O, BM						X
Helsdon and Farley 1987a,b	2D, TD, slab, O, BM	X	X	X		X	X
This study	1-1/2D, TD, kin, axi, EM, O						X

KEY:

#D : model dimension

Time dependence: SS - steady state; TD - time dependent

Model Geometry axi - axially symmetric; slab - slab symmetric

kin - kinematic model

Microphysics BM - bulk microphysics

EM - explicit microphysics

Interactions w-w - water-water; w-i - water-ice

i-i - ice-ice

O - results compared with observation

progressed toward ice-ice interactions as the primary charge separation mechanism. Many of the comparative studies (Tzur and Levin, 1981; Helsdon and Farley, 1987a) have indicated that neither the inductive or non-inductive mechanisms by themselves can explain the electrical behavior of thunderstorms. These studies have found a combination of inductive and non-inductive mechanisms is needed to provide breakdown field strengths and to have charge distributions consistent with observations. However, the parameterization of the non-inductive mechanism used in these models has not been appropriate for the ice-hail mechanism just discussed. Since modeling all the thunderstorm processes can be complex and a time expensive venture, only the most important processes are modelled explicitly while the remaining processes are parameterized. Historically, the dynamical aspects of thunderstorms have been emphasised and the microphysics simplified through parameterization. Typically, the particles are described in a few "bulk" categories with assumed particle distributions. As a result, many electrification models inherited this parameterized "bulk" microphysics. These bulk models did not incorporate the size dependence of the ice-hail charge transfer mechanism. In addition, all but one of these models have used a parameterization that neglects the observed liquid water dependence of the ice-hail charge mechanism. Thus most of these modelling efforts did not properly describe the charging characteristics of the ice-hail mechanism.

Two studies, Takahashi (1984) and Ziegler et al. (1986), used a charge per collision parameterization that depended on particle sizes. However, Takahashi did not include a liquid water dependence in his parameterization so the charge centers were associated with the highest precipitation regions of the cloud, contrary to observations. Also, Takahashi used an assumed sounding to initialize his model and did not compare his results to observations.

Ziegler et al. (1986) used a parameterization of the ice-hail mechanism proposed by Gardiner et al. (1985) to study the TRIP August 7, 1979 cloud. Unlike Takahashi, Ziegler did compare the model results with observations and the model produced fields strong enough for lightning even though these breakdown fields occurred after the observed peak flash rate of the cloud. This may be due to the fact that Ziegler used bulk microphysics with an assumed form for the particle distributions. As a result, Ziegler did not calculate the charge density directly but inferred it from assumed particle distributions. Thus it is not clear that Ziegler accurately represented the particle spectrum or charge density in the cloud. If the ice-hail mechanism is

R1/8/19

operating, large particles toward the ends of the spectrum may carry relatively large amounts of charge. Thus, the use of a realistic spectrum of hail, drop, and ice sizes and concentrations in modelling studies is important.

From this discussion it is clear that appropriate modelling studies of the ice-hail mechanism are lacking but that this mechanism appears likely to play a strong role in thunderstorm electrification. Since the charge mechanism is sensitive to particle distributions and sizes, an explicit microphysical approach should be used to study it. No model so far has incorporated explicit microphysics with a "realistic" parameterization of the ice-hail non-inductive mechanism to determine the electrical behavior of a thunderstorm, and compared the results with field observations.

1.6 Goals of this work

The goals of this work are: 1) To develop a relatively simple numerical model of the thundercloud electrification process using this non-inductive ice-hail charge separation mechanism. Since this mechanism is strongly dependent on particle size, the model will explicitly describe the hydrometeor distribution as a function of particle mass, position, and time. To maintain simplicity, a kinematic framework will be used. 2) To determine, using this model, if the non-inductive ice-hail charge mechanism can produce electric fields large enough to explain lightning initiation; and 3) To determine what parameters are important in electrification via this mechanism through sensitivity tests of both microphysical and electrical effects. The model results will be compared with observations (radar, particle distributions, charge and field measurements) to assess its performance. For this study, the Cooperative Convective Precipitation Experiment (CCOPE) July 19, 1981 storm case will be used.

1.7 Organization of this dissertation

This dissertation has six remaining parts. Chapter 2 describes the model development and outlines the assumptions used. In Chapter 3, the cloud case specifics for the base run are given. In Chapter 4, a base case model run is assessed through the comparison with observations. Chapter 5 describes the sensitivity runs. In chapter 6, a discussion of the results of the previous two chapters is given. And finally, in Chapter 7, the results are summarized and future work is suggested.

Chapter 2

Electrical/Microphysical (EM) Model Development

The ability to model the electrical, microphysical, and dynamical aspects of a thunderstorm in complete detail is beyond our current abilities. Thunderstorms have overall scales of kilometers while the charge separation and turbulent transport processes occur on scales of meters to microns. With such a vast range of scales to consider, simulations can easily become quite large and complex. Other numerical problems, such as the parameterization of turbulence, add to the difficulty. Ice, which is important in the electrification process, has a variety of complex geometries and properties, which depend on particle and cloud history, making modeling even more difficult. Therefore, modelers have relied on various simplifications in order to address the problem of thunderstorm electrification and cloud development. As shown in the introduction, many models simplify the microphysics and emphasize the cloud dynamics. Often simplifications in cloud geometry are used. Since the point of this thesis is to examine a charge separation mechanism which is strongly dependent on the particle sizes, an adequate description of the hydrometeor distributions is needed. Therefore, an explicit microphysical approach is used. To keep the problem manageable, the dynamical aspects of the modelling have been simplified by using a kinematic modelling approach. That is, the explicit microphysical and electrification equations act on velocity and temperature fields that are either retrieved from radar reflectivity patterns or taken from other cloud models. This simplification decouples the dynamics from the microphysics in the Electrification/Microphysical (EM) model described here (i.e., no feedbacks). Although feedbacks between the microphysics and dynamics are important in cumulus development, this kinematic approach provides, as I show below, an adequate framework for examining the electrical development.

Figure 2.1 shows a simple schematic of the EM model. The main inputs to the EM model are temperature and velocity fields, environmental sounding, and various parameter values. With this input, the EM model then calculates vapor density (ρ_v) and drop, ice, and charge concentrations (n_d , n_i , and ρ_c) as functions of

$T(z,t)$ and $w(z,t)$
Environmental sounding
Parameter values



Electrification/Microphysical (EM) Model

Processes

Deposition Growth of Drops and Ice

Collection/Electrification

Ice Formation



$\rho_v(z,t)$, $n_d(m,z,t)$, $n_i(m,z,t)$, and $\rho_c(m,z,t)$

Figure 2.1: EM model schematic with inputs and outputs.

mass, height, and time. Charge is associated with individual particle classes. Three microphysical processes are included; deposition, collection, and ice formation. Since the electrification is linked directly to ice particle collisions, collection and charge transfer are done at the same time. The details of these processes are described below. The advantage of our explicit microphysical model over those which use parameterized microphysics (e.g., Ziegler et al., 1986; Helsdon and Farley, 1987a), is that the particle distributions and the charge per particle are computed directly. Thus the size dependence of charge concentration can be examined.

In order to reduce computation time, fall velocities, depositional growth rate factors, and collection kernels (described below) are calculated assuming a single temperature profile. This simplification is reasonable since the in-cloud temperatures only vary by a few degrees over the cloud lifetime at most grid points. Model runs using a different temperature profile showed only minor differences in the calculated results. However, the time-varying temperature profile is used for processes (e.g., ice formation) in which temperature effects are especially important.

2.1 Model geometry and advection scheme

Since the temperature and velocity fields used for this kinematic case study were generated from the 1-1/2 dimensional, time-dependent, Eulerian cloud model of Taylor (1987, 1989, referred to hereafter as T), the EM model uses the same geometry. The T model was developed to examine the dynamical, thermodynamical, microphysical, and chemical processes within low shear, mid-latitude, continental cumulus clouds and is describe in more detail in the next chapter. The model geometry, as shown in Figure 2.2, consists of a cylindrical core (called the inner region) encased in a cylindrical annulus (called the outer region) and surrounded by a time-independent environment. The radius of the inner region is 1.0 km while the radius of the outer region is 2.5 km. The vertical grid spacing is 200 m.

The T model computed the temperature and velocity fields at approximately 60 second intervals; therefore the EM model updates these fields every 60 seconds. Between updates, these fields are assumed to be constant in time. The error introduced by this approximation has little effect on the model results since a test run using 30-second update intervals produced nearly identical results to the 60-second case.

Because the EM model uses the same geometry as the T model, the EM model

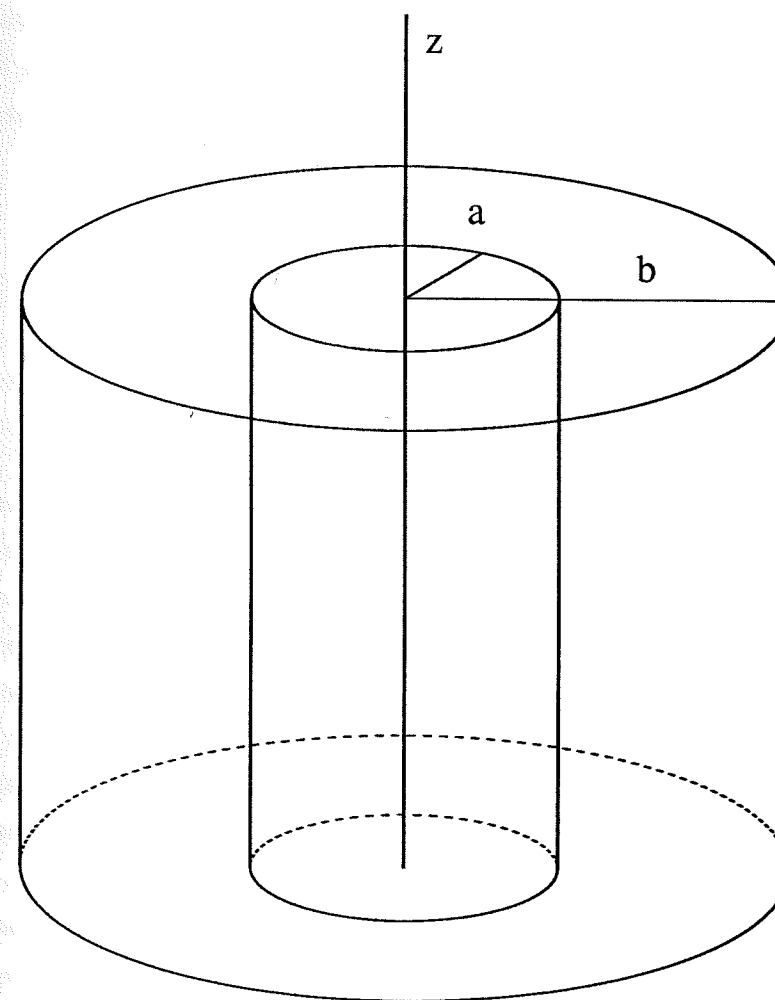


Figure 2.2: The model geometry showing the inner and outer regions.

incorporates the same generalized area-averaged advective equations as T with several modifications (Derivation of these equations and further description of the terms are provided in Appendix A). The basic area-averaged advective equations for generalized densities in the inner region (ρ_i) and outer region (ρ_o) are

$$\frac{\partial \rho_i}{\partial t} = -\frac{\partial(\omega_i \rho_i)}{\partial z} - \rho_a \frac{\partial w_i}{\partial z} - \frac{2}{a}(\rho_i' u')_a - \frac{\partial}{\partial z}(\omega_i' \rho_i') + S_{e_i} \quad (2.1)$$

$$\begin{aligned} \frac{\partial \rho_o}{\partial t} = & -\frac{\partial(\omega_o \rho_o)}{\partial z} + \left[\rho_b \frac{\partial w_o}{\partial z} + (\rho_b - \rho_a) \frac{a^2}{(b^2 - a^2)} \frac{\partial w_i}{\partial z} \right] + \\ & \frac{2a}{(b^2 - a^2)} (\rho_i' u')_a - \frac{\partial}{\partial z}(\omega_o' \rho_o') + S_{e_o} \end{aligned} \quad (2.2)$$

where ω_i and ω_o are the inner and outer region vertical air velocity for the vapor and the difference between the air and fall velocity for particles. The densities at the inner-outer boundary and outer-environment boundary are designated ρ_a and ρ_b , respectively. Deviations from the mean are designated by primes. The terms on the rhs of equations 2.1 and 2.2 are the vertical advection, dynamic entrainment, lateral eddy flux, vertical eddy flux, and a generalized source/sink term. The outer region/environment lateral eddy flux term, which is not shown, has been set to zero in the model for simplification. To examine the effect of intra-cloud mixing, a constant (values of 1 or 1/3) was added to the eddy diffusivity as shown in Appendix A.

The numerical advection scheme is that of Smolarkiewicz (1983,1984) with two corrective steps to solve

$$\frac{\partial \rho}{\partial t} + \frac{\partial}{\partial z}(w \rho) = 0. \quad (2.3)$$

This advective scheme is an upstream, first order, finite difference approach with anti-diffusive corrective steps. It is simple and positively defined (i.e. positive quantities always remain positive); however it does produce small ripples (<10%) near sharp gradients.

Since only the advective equations, like those shown above, are geometry dependent, the EM model can easily be adapted to other geometries.

2.2 Particle characteristics

2.2.1 Mass grid

The size distributions for all particles (drops and ice) are defined on a mass grid following Berry (1967). The mass of particles in the k th category is

$$M_k = M_o 2^{\frac{(k-1)}{2}} \quad (2.4)$$

where M_o , the mass of the lowest category, is that of an ice sphere with a 5 micron radius. The mass doubles every second category. There are 30 size categories of drops and 78 of ice.

2.2.2 Ice density parameterization

Each ice category has a pre-set ice density associated with it. This is a common simplification in explicit microphysical models (Hall, 1980; Takahashi, 1984; Farley and Orville, 1986). Also, all particles are assumed spherical. Although this assumption is probably reasonable for larger ice particles ($D > 1$ mm), the smaller ice particles are not spherical but have a variety of shapes (plates, dendrites, columns). Trying to incorporate all these shapes into the model would be computationally inefficient. To compensate, the ice crystal density (ρ_{crys}) is set to a relatively low value (0.1 g-cm^{-3}) since the diameter of a sphere would be less than that for of a plate or dendrite of the identical mass. The value of 0.1 g-cm^{-3} was selected based on estimates of the ice crystal density needed to give a sphere the same radius as an plate with the same mass and on estimates of the snow density used by T (see Appendix B). Ice crystals (i.e. non-riming particles) have diameters less than a critical riming diameter (D_r). For diameters above D_r , the density of particles of mass M_f is determined iteratively by

$$\rho(M_f)(\text{g-cm}^{-3}) = \rho(M_d) + \int_{M_d}^{M_f} \left(1.0 - \frac{\rho(M)}{\rho_a(M)}\right) \frac{dM}{Vol(M)} \quad (2.5)$$

M_d is the mass of a particle of diameter D_r , Vol is the volume of the particle, and ρ_a is the density of the accreted rime. The EM model has three forms for ρ_a which produce light, medium, and dense rime, respectively. Specifically,

$$\rho_a(\text{g-cm}^{-3}) = \begin{cases} \rho_{light} = 0.11A^{0.76} \\ \rho_{medium} = 0.30A^{0.40} \\ \rho_{dense} = 0.90 \end{cases} \quad (2.6)$$

where

$$A = \frac{-rV_{imp}}{T_c} \quad (2.7)$$

where $r(\mu)$ is the radius of the cloud drops and $V_{imp}(m-s^{-1})$ is their impact velocity on a target with surface temperature $T_c(^{\circ}C)$. For the EM model, A was determined assuming that $T_c = -10^{\circ}C$, $r = 10\mu$, and V_{imp} is the riming particle terminal fall velocity. Thus, A is a function of the particle mass.

The light density case is based on the experiments of Macklin (1962) who studied the riming behavior of a cylinder to simulate hailstone growth over a wide range of conditions. The medium density case, which has the same general form as the light density expression, was derived by Heymsfield and Pflaum (1985) when they re-analyzed the Pflaum and Pruppacher (1979) data for the riming behavior of free falling graupel. Hail modelers tend to use Macklin's form while those examining graupel development favor the Heymsfield and Pflaum forms (Farley, 1987).

2.2.3 Fall velocities

The particle fall velocities are determined from the Reynolds number (Re) and drag coefficient (C_d) (Berry and Pranger, 1974; Pruppacher and Klett, 1978). The relationship between Re and C_d is expressed as an empirical function of $C_d Re^2$, (commonly referred to as the Best number (X)) which is dependent only on the particle mass and the atmospheric conditions (i.e., T and P). For ice particles with X greater than 400, I use the empirical expressions of Heymsfield (1978), derived from an analysis of summertime graupel collection data of Auer et al. (1971). Since the Heymsfield form is not appropriate for the smaller ice particles, the Berry and Pranger (1974) formulation for solid spheres for ice is used. The switch-over point ($X = 400$) is where the two formulations give similar values for Re . The fall velocities of drops are modeled using the Berry and Pranger formulation.

2.3 Microphysical equations

2.3.1 Deposition

Both drops and ice particles grow by vapor deposition. Deposition is modeled using the classical explicit expression for spheres growing in a constant vapor field assuming a steady state condition in which the heat release due to vapor deposition to the

sphere is balanced by the heat conducted away from the sphere (Pruppacher and Klett, 1978). Ventilation factors (f_α , f_β , f_T , and f_v) are added to account for air motions about the particle (Young, 1974). The depositional growth rate is given by:

$$\left. \frac{dm}{dt} \right|_{dep} = \frac{4\pi r S^*}{D \frac{1}{\rho_s^* f_\beta f_T} + \frac{L^*}{KT f_\alpha f_v} \left(\frac{L^*}{R_v T} - 1.0 \right)}. \quad (2.8)$$

The starred variables (S- the supersaturation, L (ergs/g) - latent heat, ρ_s - saturated vapor density) take on two sets of values for liquid and solid particles; D ($cm^2 s^{-1}$) is the diffusion constant for vapor, and R_v (erg/K) is the gas constant for water vapor. Only S is calculated during the iterative phase of the model while the remaining factors are calculated beforehand.

The depositional growth equation for $n(m)$, the number concentration (cm^{-3}) of particles of mass m , is

$$\frac{dn(m)}{dt} = -\frac{d}{dm}(n(m)u_m) \quad (2.9)$$

where $u_m \equiv \partial m / \partial t$. Equation 2.9 has the form of the advection equation 2.3 where u_m is analogous to the velocity in a spatial framework (Hall, 1980). Thus an advection scheme, like that of Smolarkiewicz (1984), can be used for equation 2.9. The scheme is stable when the Courant number ($X_{CN} \equiv u_m \Delta t / \Delta m$) is less than 1 for non-divergent flow, where Δt is the time step and Δm is the width of the mass category. When ice is nucleated in the presence of drops the advective scheme often becomes unstable for the low mass categories because Δm is small and the growth rates (u_m) are high. To make the scheme stable, either the time step would have to be reduced, and sometimes considerably, thus increasing the computation expense, or another approach used. I have devised a hybrid calculation method rather than reducing the time step. I use a Lagrangian method in the unstable regions of the grid and the Eulerian advection scheme in the stable regions. In the Lagrangian scheme, the time it takes a particle to grow through a category is determined, given the supersaturation, for each category. If a particle grows through a category, the mass that the particle acquires is simply equal to the mass width of the category. For particles that grow only part way through a category, the mass acquired is equal to the growth rate multiplied by the time spent in that category. Thus the total mass gained in a time step by a growing particle is found by summing the mass accumulated in all categories partially or completely traversed in that time step.

The particles are then redistributed back onto the grid, as shown below, so as to conserve both number concentration and water content. Since the mass "flow" tends to converge toward larger masses, particles from these unstable, low-mass categories tend to stay closely grouped, usually within several categories, using this method. This Lagrangian scheme is not used for the entire grid. In the low Courant number (stable) areas of the grid where only a fraction of the particles are advancing into the next category, diffusion effects due to the redistribution of particles back to the grid become important. Thus the Eulerian scheme, which is designed to limit such diffusion, works better in the stable regions.

2.3.2 Particle redistribution

The redistribution process is used in the Lagrangian depositional growth described above and in the collection routine below. After these processes are performed, a group of particles with concentration n and final mass M must be placed back onto the mass grid. It is extremely rare that M is equal to the characteristic mass of a category; rather M usually lies between two mass categories so that $M_i < M < M_{i+1}$. Therefore, the concentration of these particles must be divided between the two mass categories in order to conserve both the total particle number concentration and water mass. Conservation of number concentration requires

$$n = n'_i + n'_{i+1} \quad (2.10)$$

where n'_i is the particle contribution to the i^{th} category and n'_{i+1} is the contribution to the $i + 1$ category. Likewise, mass conservation gives

$$nM = n'_i M_i + n'_{i+1} M_{i+1}. \quad (2.11)$$

Since there are two equations and two unknown, solutions for both n'_i and n'_{i+1} are easily obtained. Solving for n'_i gives

$$n'_i = \frac{M - M_{i+1}}{M_i - M_{i+1}} n. \quad (2.12)$$

2.3.3 Particle interactions: collisions and collection

Both the microphysical and electrical aspects of the cloud are dependent on the number and type of particle interactions. Riming ice particles grow by collection of

smaller ice particles and drops while the amount of electrification is dependent on the number of separating ice-hail collisions. Therefore, the total number of collisions a particle undergoes and the amount of subsequent collection must be determined.

The number of collisions that larger particles have with a population of smaller particles is determined using a "continuous collection" approach. This approach assumes all large particles of the same size have the same number of interactions (Gillespie, 1975). This is very similar to the Lagrangian depositional scheme described above. Particles with diameters greater than D_r collide with drops and smaller ice particles. The number of collisions a particle has with the population of smaller particles in a time step dt is:

$$N_{collisions} = n_{small} K_{cc} dt \quad (2.13)$$

where n_{small} is the concentration of smaller particles and K_{cc} is the collision kernel. In this study, the geometric collision kernel (K_{cc}) is used and is defined as

$$K_{cc}(d, D) = \frac{\pi}{4} (D + d)^2 |\Delta v| \quad (2.14)$$

where D and d are the diameters of the large and small particles and Δv is the difference in the particle fall velocities. Thus the number of collision is equal to the number of small particles in the volume swept out by the large particle in a time dt .

The number of collections a particle has is the number of collisions times the efficiency of sticking (E_{si}). The collecting particles retain the mean characteristics of the starting category over each time step. After collection is complete, the particles are redistributed on the mass grid as described in the last section.

For drop-ice interactions, I assume all collisions result in collection ($E_{si} = 1$). However, for ice-ice interactions, this assumption does not hold. Deshler and Vali (1985) estimated a collection efficiency of a few percent for dry growth regions. This dry growth condition seems appropriate for our study since graupel sizes were in the millimeter range with moderate liquid water contents ($\leq 3.0 \text{ g-m}^{-3}$). On the other hand, Keith and Saunders (1989) estimated that 90% of the 100μ ice crystals were collected by their 'rimer'. However, it is not clear how to relate the long cylindrical geometry, and hence collection efficiencies, of the rimer to more spherical particles in clouds. Thus, there is a significant uncertainty in how to select the collection efficiency. In this model, two assumptions are made. First, the largest

riming particles do not collect other large riming particles. In other words, only ice particles with diameters less than a critical value (D_{crit}) can be collected. The further significance of D_{crit} is given in the electrification section below. The second assumption is that the ice-ice collection efficiency is a constant, independent of the size of the ice crystal or riming particle. The sensitivity of the electrification to the ice-ice collection efficiency (E_{si}) is examined later.

In the current version of the EM model, the large drop microphysical processes (i.e. coalescence, breakup) have been simplified or excluded. This was done because these large drop processes did not contribute in the cloud case (CCOPE July 19, 1981) examined here. Aircraft observations found no drizzle-type precipitation even though liquid water mixing ratios exceeded $4 \text{ g}\cdot\text{kg}^{-1}$ ($2.5 \text{ g}\cdot\text{m}^{-3}$ at 500 mb, $T=-20^\circ\text{C}$) (Dye et al., 1986). This can be attributed to the cold cloud base ($\approx 1^\circ\text{C}$), continental drop concentrations ($600\text{-}800 \text{ cm}^{-3}$), and a narrow drop spectrum ($\sigma \approx 1.3\mu$) (Jensen et al., 1985). These observations lead Dye et al to suggest that graupel development in this storm occurred primarily through the ice phase. Furthermore, the T model incorporated the effect of drop concentration in the autoconversion formulation and found that an autoconversion threshold of $5.75 \text{ g}\cdot\text{kg}^{-1}$ was needed to initiate rain via coalescence in the July 19 case. Since the model mixing ratios never reached $5.75 \text{ g}\cdot\text{kg}^{-1}$, rain development through coalescence was not a significant process in the modelled cloud. Because both observations and modelling efforts have indicated that coalescence was not important in the July 19 storm, limiting the warm cloud processes for this case study is justified. However, drop coalescence and other warm cloud processes will have to be added for future warm cloud based studies. As a result, drop coalescence is currently approximated in the EM model as a simple drop-drop collection scheme which uses the same formulation as the ice collection described above. This drop-drop collection assumes a stick efficiency of unity and a minimum collection diameter (analogous to D_r) of 20 microns.

2.3.4 Ice formation

Since the non-inductive charge transfer process relies on ice-ice collisions for the separation of charges, proper description of the ice formation processes is important for its realistic representation. Primary nucleation is assumed to follow the empirical

relations of Fletcher (1962) where the ice nucleation concentration is given by

$$IN(\text{cm}^{-3}) = \alpha e^{\beta(T_0 - T)} \quad (2.15)$$

where α (typically set to 10^{-8} cm^{-3}) and β are constants and T_0 is 273.16 K. Typically β is set to 0.6; however, T used $\beta = 0.5$ for his base run. Entrainment of IN (in concentrations given by the Fletcher relation) occurs at cloud sides and at cloud top, with subsequent upward and downward transport. Drop freezing is incorporated by assuming half of the activated IN are in drops. At -40°C , all drops freeze spontaneously.

There are other ice formation processes that I have not included here. Although the model does include a parameterization for the Hallett-Mossop ice multiplication process (Harris-Hobbs and Cooper, 1987), it has not been used in this case study since the conditions for this process (large drops in the -3°C to -8°C temperature range) are not present in cumulus clouds in the CCOPE region (Mossop, 1978; Heymsfield et al., 1979; Dye et al., 1986). Other modelling studies (Knight, 1990) of the July 19 storm have indicated that primary ice nucleation was sufficient to explain the observed ice concentrations. Hobbs and Rangno (1985) have shown that clouds with relatively warm tops can have considerably larger ice concentrations than those predicted by primary ice nucleation. However, this ice enhancement is not observed in continental cumulonimbus, such as the CCOPE cloud I investigate here, so I have not attempted its parameterization in this study. A final ice formation possibility also neglected is that ice particles from previous storms are entrained as a cloud grows through the storm debris (Ziegler et al., 1986).

2.4 Electrification equations

As mentioned before, the amount of electrification is dependent on the number of separating collisions between small ice particles and larger graupel or hail particles. The net amount of charge added to a graupel particle colliding with a population of smaller ice crystals of diameter d is given by

$$\begin{aligned} \Delta Q(d, D) = & n_{small}(d)K_{cc}(d, D)(1.0 - E_{si})\delta q(d, D) \\ & + Q_{small}(d)n_{ice}K_{cc}(d, D)E_{si} \end{aligned} \quad (2.16)$$

where δq is the charge transferred per collision to the larger particle and $Q_{ice}(d)$ is the charge per small ice particle. The first term is the charge transferred as a result

of rebounding collisions and the second term is the contribution of charge which was on the small particles that were collected.

In a series of laboratory experiments on charge transfer in ice-hail collisions, Keith and Saunders (1989) obtained the results shown in Figure 2.3. For the small ice crystals, the charge magnitude was proportional to d^4 , in agreement with the original results of Jayaratne et al. (1983). However, this dependence falls off for the larger crystal sizes. Also, the magnitude of the positive charging to hail, which occurs at temperatures warmer than T_r , is larger than the negative charging magnitudes. From these recent data, a parameterization of this charge mechanism was made that is similar to that proposed by Gardiner et al. (1985). The charge (δq) transferred to a large particle (diameter D) via collision with a small particle (diameter d) is

$$\delta q(d, D, lwc, T) = S(T)\mathcal{R}(d, D, lwc)\mathcal{M}(d, D, T) \quad (2.17)$$

where S determines the sign of the charge transferred, \mathcal{R} is a restriction function and has values of 0 or 1, and \mathcal{M} is the magnitude of the charge transferred.

The sign function S is only a function of T and is given by

$$S(T) = \begin{cases} -1, & T < T_r \\ 0, & T = T_r \\ 1, & T > T_r \end{cases} \quad (2.18)$$

where T_r is the reversal temperature and is set at -15°C .

The restriction function \mathcal{R} determines whether or not the charge process is active and is given by

$$\mathcal{R}(d, D, lwc) = \theta(lwc - lwc_c) \theta(D - D_r) \theta(D_{crit} - d). \quad (2.19)$$

where θ is a step function: $\theta(x) = 0$ for $x < 0$ and $\theta(x) = 1$ otherwise. The first θ function is zero if the liquid water (lwc) falls below a critical value (lwc_c) set at 0.1 g-m^{-3} . This function describes the liquid water dependence of the charge mechanism. Since D_r is the minimum diameter for riming particles, the second θ function states that the larger of the two particles must be undergoing riming. The role of the last θ function is less obvious. The experiments with the charge separation mechanism suggest the difference in the surface properties of the colliding ice is important for charge transfer (Baker et al., 1987; Baker and Dash, 1989).

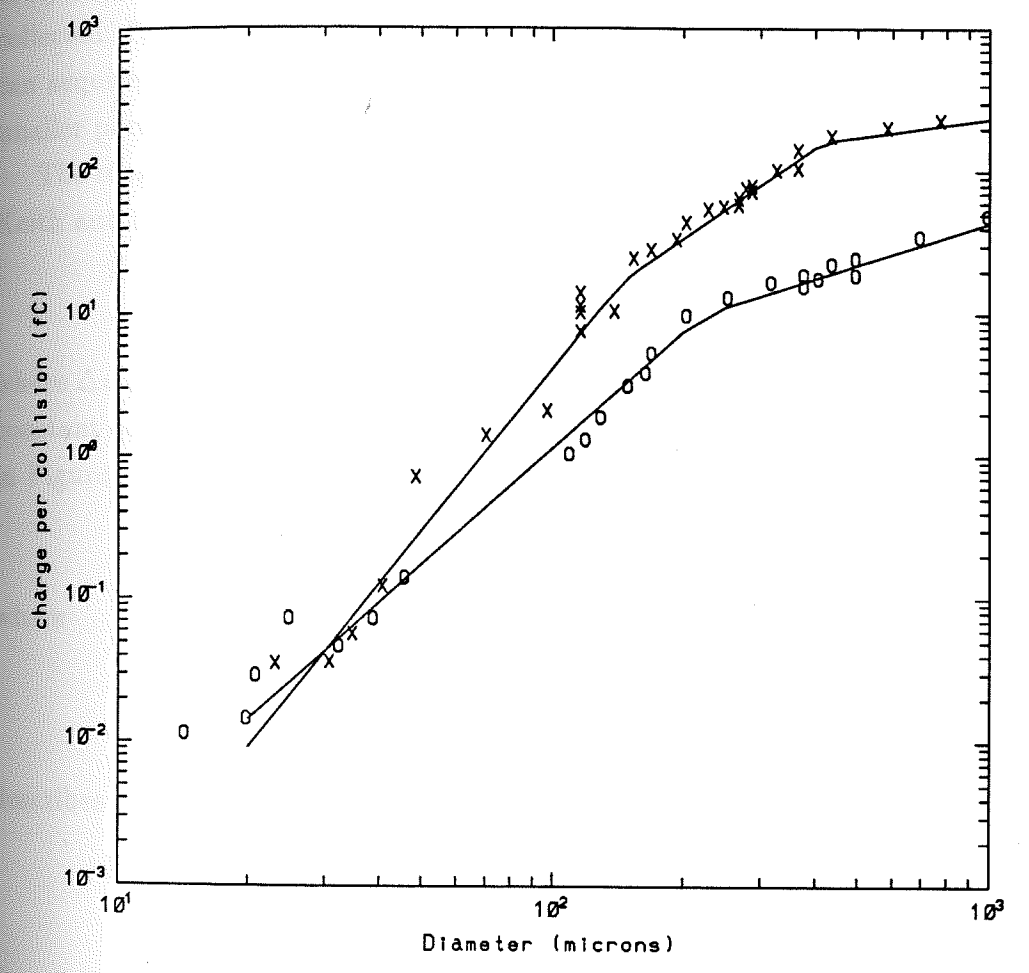


Figure 2.3: Charge transferred per collision vs. small crystal diameter. The X's and O's are positive and negative charging data from Keith and Saunders (1989). The piece-wise linear fits are the parameterizations for the model.

Under this assumption, colliding ice particles with similar surface properties may not separate much charge. However, this case has not been well defined by experiments. Therefore, the parameter D_{crit} is used to distinguish the 'large' particles which are growing primarily by riming from the 'smaller' particles growing by vapor deposition or by vapor deposition and riming. Particles with diameters less than D_{crit} can be collected. Note that if D_r is less D_{crit} , particles with diameters between D_r and D_{crit} can acquire both positive and negative charge via collisions with larger particles and smaller particles. The effects of D_{crit} on the electrification will be discussed later.

The magnitude of the charge transferred (\mathcal{M}), in fC, is a parameterization of the Keith and Saunders data and is given by

$$\mathcal{M}(d, D, T) = \left| \frac{\Delta v}{\kappa} \right|^{2.5} G(d, T) \quad (2.20)$$

where Δv (m/s) is the difference in the large and small particle fall velocities, κ is a constant equal to 3.0 (m/s), and G (fC) is the piece-wise linear fit of the data shown in Figure 2.3:

$$G(d, T) = \begin{cases} G_+(d), & T \geq T_r \\ G_-(d), & T < T_r \end{cases} \quad (2.21)$$

where

$$G_+(d) = \begin{cases} 10^{-6.98}(d)^{3.8}, & d \leq 133\mu \\ 10^{-3.35}(d)^{2.12}, & 133 < d \leq 435 \\ 10^{1.08}(d)^{0.43}, & 435 < d \end{cases} \quad (2.22)$$

describes the positive hail charge behavior and

$$G_-(d) = \begin{cases} 10^{-5.38}(d)^{2.7}, & d \leq 222\mu \\ 10^{-1.30}(d)^{0.98}, & d > 222\mu \end{cases} \quad (2.23)$$

describes the negative hail charging. This parameterization provides a reasonable approximation to the Keith and Saunders (1989) curves for this non-inductive mechanism.

2.5 Model limitations and omissions

As mentioned, some warm microphysical processes (coalescence, drop breakup) have been excluded because they were not applicable to the cloud case examined in this study. Next, snow and aggregate processes have been neglected. This could well be

an unreasonable assumption for this cloud case; however the incorporation of snow into the mass grid scheme would not be a straightforward process. Since one of the goals of the model was simplicity, snow was approximated by setting the ice crystal density to 0.1 g-cm^{-3} . In order to generate realistic, time-dependent ice distributions, our model domain extends from about the -1°C level to just below the maximum cloud top. I assume that only drops enter from below, during periods of updrafts, and that their cloud base distribution is time independent. Thus the recycling of precipitation from below the freezing level is assumed negligible. This assumption is supported by observation and the model since the duration of the storm was short. Finally, electrical effects like corona, lightning currents, and other phenomena are not considered. Also, no parameterization for lightning is included since I am concerned primarily with the early electrical development of the storm. These simplifications to the model, with the possible exception of the neglect of snow processes, generally should not affect the performance of the model, as applied to the case study.

Chapter 3

Base Case Description and EM Initialization

3.1 Description of CCOPE July 19 case study

For this study I have used the Cooperative Convective Precipitation Experiment (CCOPE) July 19, 1981 southern Montana cloud case which has been well documented (Gardiner et al., 1985; Dye et al., 1986). The cloud was a small, isolated cumulonimbus. At the onset of the experiment, cloud base was at 3.9 km (1°C) and cloud top at 6.5 km (-20°C). Two turrets grew out of the cloud top with the NE one dominant. This dominant turret grew to a height of 10.5 km and subsequently formed an anvil. The cloud had one intra-cloud discharge, as inferred by a sharp discontinuity in the sailplane horizontal electric field measurement (Dye et al., 1986).

3.2 Background model

As mentioned before, the temperature and velocity fields used for the kinematic case study described here are generated from the 1-1/2 dimensional, time-dependent, Eulerian cloud model of T. This model was developed to examine the dynamical, thermodynamical, microphysical, and chemical processes within low shear, mid-latitude, continental cumulus clouds. As mentioned in the last chapter, the model geometry consists of an inner, outer, and environmental regions. Mixing occurs between the inner and outer regions and between the outer region and the environment. The mixing rates are parameterized in terms of an eddy diffusivity that depends on the local turbulence intensity and a buoyancy modified mixing length. Subcloud forcing consisted of a pre-specified updraft at and below an input cloud base level in both the inner and outer regions for a selected length of time. The height profile of the vertical velocity below cloud base was given by

$$w_c(z \leq z_{cb}) = w_{cb} \frac{z}{z_{cb}} \quad (3.1)$$

where z_{cb} and w_{cb} are the cloud base height and vertical velocity values. Midway through the forcing, the inner region cloud base vertical velocity was multiplied by 1.5 or 2. T increased the inner region vertical velocity to reduce the cloud base entrainment and produce a more adiabatic inner region updraft core. At and below cloud base, the advected quantities were set to cloud base values and were fixed for the entire forcing time. When the forcing ended, the sub-cloud moisture and energy were returned to the environmental values. To damp the initial discontinuity at cloud base, the initial vertical velocity and moisture above cloud base were given by

$$w_c(z, t = 0) = w_{cb} e^{-\left[\frac{(z-z_{cb})}{b \text{ radm}}\right]^2} \quad (3.2)$$

$$q_v(z, t = 0) = q_s(z) e^{-\left[\frac{(z-z_{cb})}{b \text{ radm}}\right]^2} \quad (3.3)$$

where w_{cb} is the cloud base velocity, q_s is the environmental saturated mixing ratio at height z , z_{cb} is the cloud base height, b is the radius of the outer region, and radm specifies the depth of the perturbation. T used values of 0.1 to 0.3 for radm which resulted in perturbed fields for about 2 to 3 levels above cloud base. T used bulk microphysics with four particle categories (cloud drops, precipitation, snow, and graupel). The microphysical parameterization includes a Kessler (1969) form for autoconversion, a Cotton (1975) form for the collection, and the Cheng (1981) modification of the Stephens (1979) forms of the ice phase. The model was extensively tested, using the CCOPE July 19, 1981 case (T).

The Miles City sounding, which was closest to the storm in time and space, was used as input to initialize the T model run from which the temperature and velocity fields were computed. Figure 3.1 shows the vertical velocity field as a function of time and height for the inner and outer regions. The figure time scale begins at 1565, increments every 60 seconds, and ends at 3545. The model cloud initially grew to about 7.0 km (-20°C) and remained there for about 1000 seconds. Downdrafts develop in the outer region, due to evaporative cooling and mass continuity constraints. At about the 2400 second mark, the cloud began a rapid growth. A maximum updraft of 12 m/sec occurred at 2700 seconds, in good agreement with observations. Once cloud top was reached the cloud began to subside. At 2700 seconds, the sub-cloud forcing ended and downdrafts started in the lower portions of the cloud due to precipitation loading. Table 3.1 shows a summary of comparisons of the observations (Dye et al. (1986)) with the results of the T model. Dynamically,

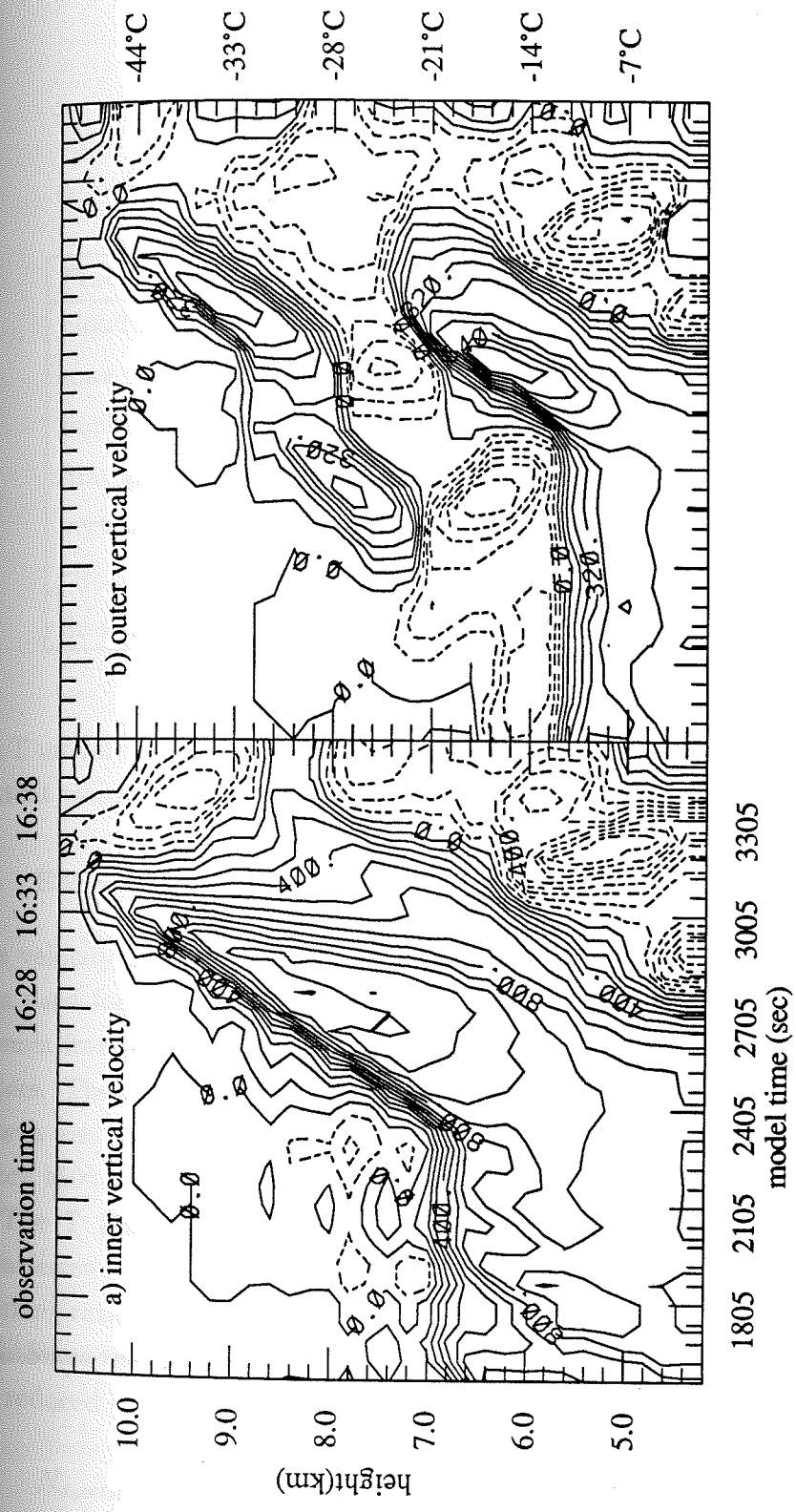


Figure 3.1: Inner and outer vertical velocities from model times 1565 to 3545 as input to the EM model. Contour levels are every 100 cm s^{-1} . Solid lines represent upward vertical velocities while dashed lines are downward velocities.

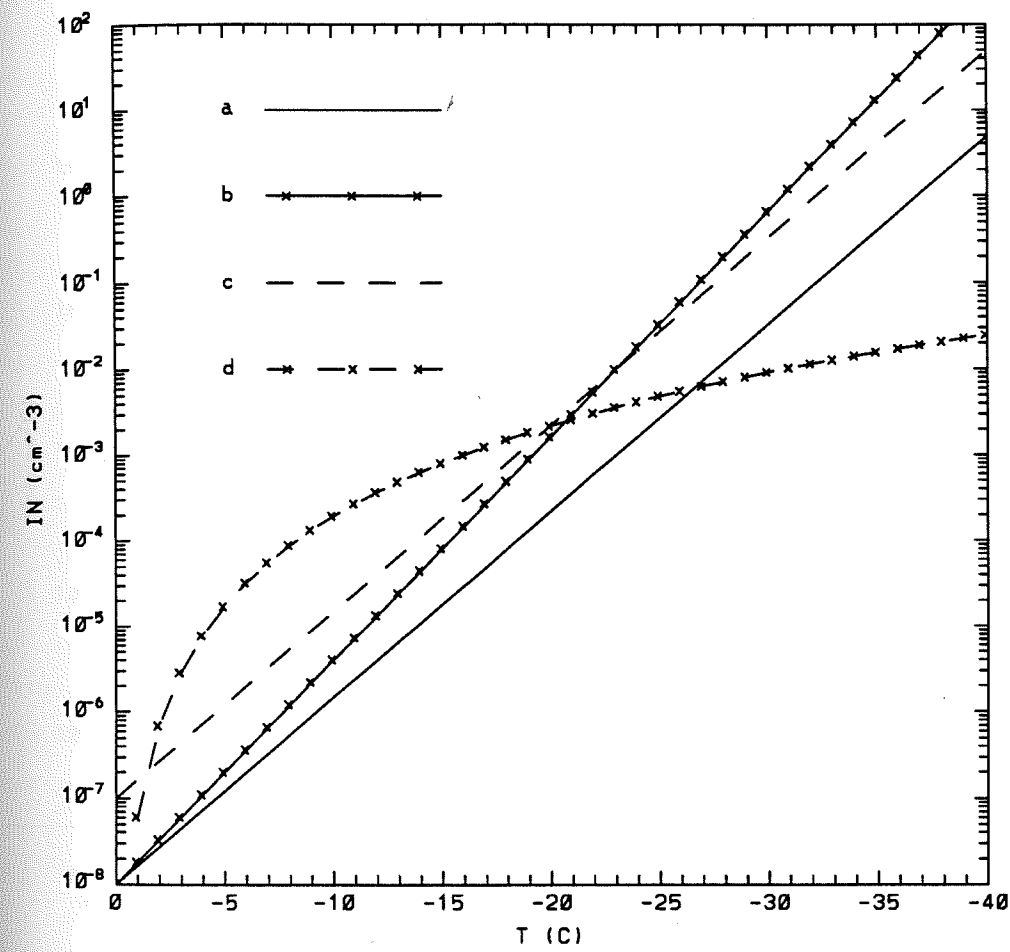


Figure 5.6: Ice nucleation concentrations (cm^{-3}) vs. temperature for the four ice nucleation runs. Letters correspond to the runs defined in Table 5.4.

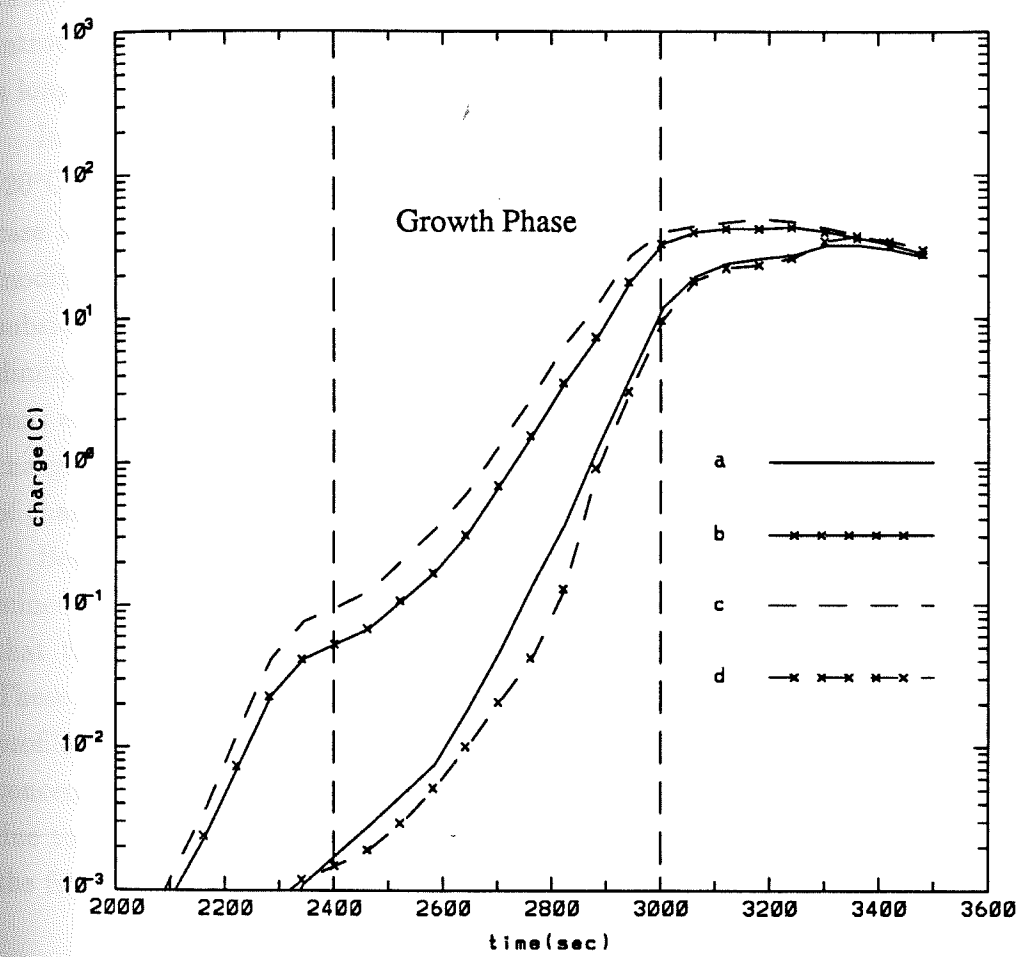


Figure 5.7: Total negative charge in the inner region for the ice nucleation runs.

After 3000 seconds, the total amount of negative charge in the inner regions stabilizes as the cloud glaciates and then subsides. In the low ice runs, the charging is delayed. However, charging continues until 3400 seconds when the cloud completely glaciates. By the time the clouds have completely glaciated, the total negative charge in all the runs is similar. Thus the primary difference in these runs is that the high IN runs introduce more ice into the lower portions of the cloud earlier so these particles have a longer exposure to the liquid water needed for charging.

In the kinematic framework of this model, the amount of water available above -20°C is dependent on the velocity profiles which are fixed. This would not be the case in a real cloud or a dynamical model in which microphysical feedbacks would modify the velocity and vapor fields. Therefore, if the velocity fields in the EM model subsided before the full glaciation effects occurred, the amount of charging would be diminished. This appears to be the case in the low EM ice nucleus concentration runs suggesting that these low IN runs may be underestimating the total amount of charge separated. Thus the velocity fields themselves put constraints on the amount of charging.

Besides the temporal aspects of the charging, the IN parameterization also determined the location of the main negative charge center. In the last chapter I showed that the location of the negative center was associated with the MPG interface. These runs exhibited the same behavior. Figure 5.8 show the net charge density profiles for each of these IN runs. Note that runs a and d, which have the lower IN concentrations, have higher negative charge centers than the high IN runs. This is due to the lower level of glaciation in the high IN runs. Also, as suggested before, the first occurrence of the $1\text{ nC}\cdot\text{m}^{-3}$ contour appears earlier in the high IN runs.

5.3 Mixing

To determine the effects of intra cloud mixing on the electrical development of the model cloud, the mixing constant (α_m , see Appendix A) was increased from $1/3$ to 1. The primary effect of the increased mixing can be seen in the net charge density time-height profile (Figure 5.9). The main negative charge region is now between -21 and -28°C rather than above -28°C . The upper charge region still exists (due to the freezing of drops) but it is dwarfed by the lower region. Thus it appears that mixing established this main lower charge region as high concentrations of particles

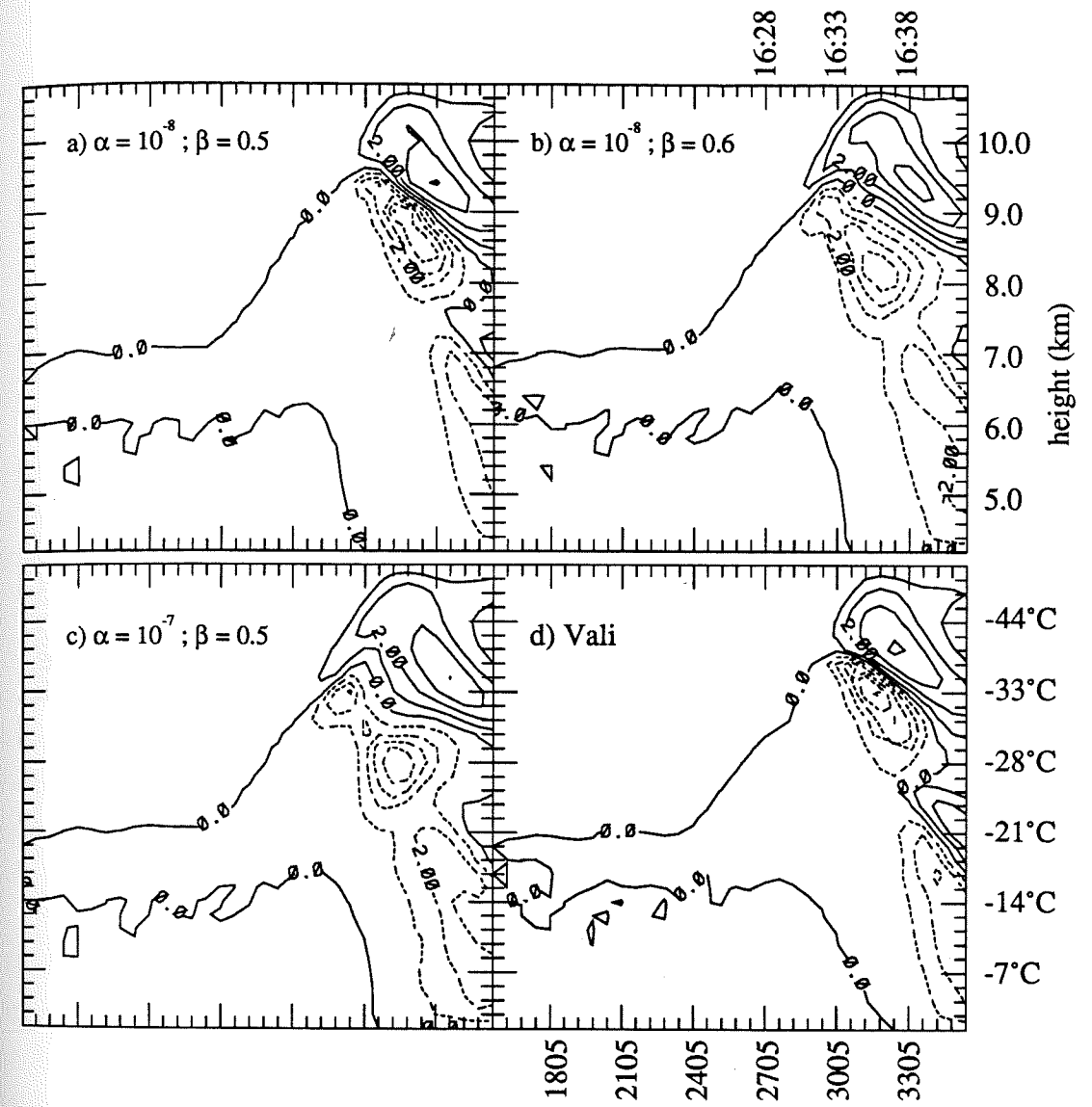


Figure 5.8: Time-height profiles of the inner region net charge density for the ice nucleation runs.

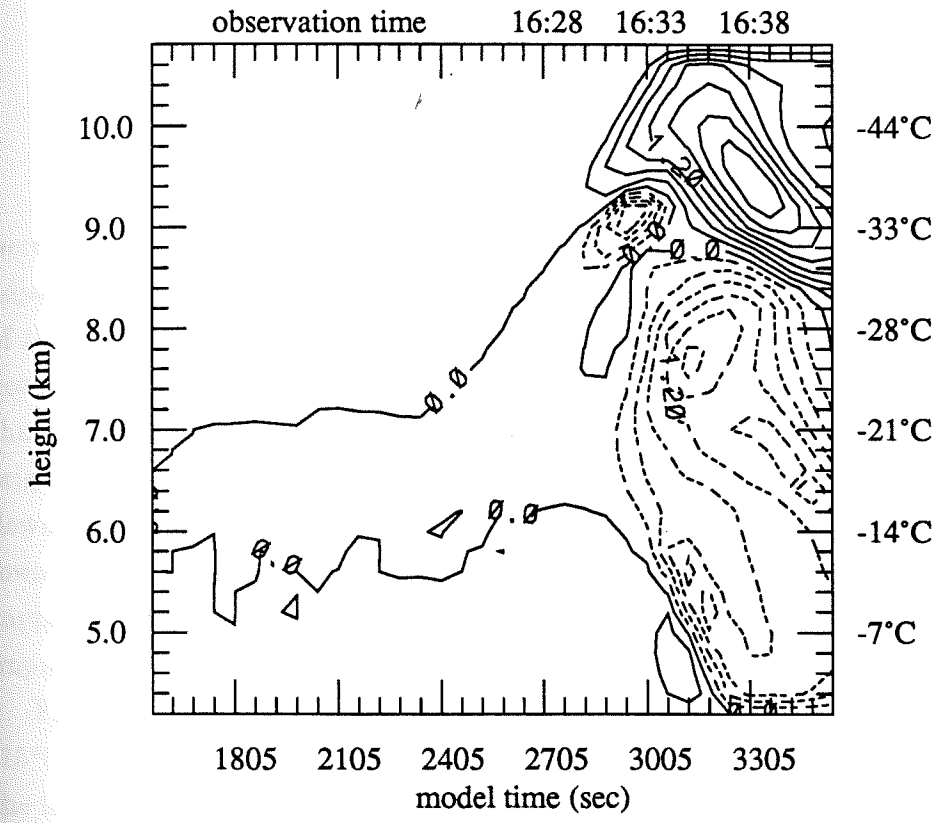


Figure 5.9: Time-height profile of the net charge density for the enhanced mixing run. Contour levels are $0.3 \text{ nC}\cdot\text{m}^{-3}$.

Table 5.5:

Mixing run summary

	Maximum magnitudes for		
	dBZ_e	Q_{ntot} (C)	E_a (kV-cm ⁻¹)
Base	49.2	32.38	2.34
Mixed	43.8	35.77	1.27

were 'mixed' there. The turbulent eddy mixing includes both vertical mixing between adjacent height levels and lateral mixing between the inner and outer region. Because of the the strong inner region updraft, the inner region vertical eddy mixing could not mix these high concentrations of ice to the lower levels. Thus, the lower negative charge center is primarily the result of higher concentrations of ice particles which originated at colder temperatures and were transported downward in the outer region downdrafts. These higher concentrations of ice were then mixed back into the the lower portions of the inner region by the lateral mixing (and entrainment). This result supports the Dye et al. (1986) suggestion that the updraft/downdraft interface is important in establishing the lower negative charge center.

Figure 5.10 shows the charge per particle at 3400 seconds and $z = 5.8$ km ($T \approx -15^\circ\text{C}$). Panel a shows the base run; the smallest particles carry positive charge and the larger ones carry negative charge since charging primarily occurred above -15°C . However, in the enhanced mixing run, there are three different groups of charge carriers. As before, the largest particles carry negative charge from charge transfers which occurred at heights above -15°C . However, the 1.0 to 2.1 mm sized particles are charged positive and the small particles ($D < 1.0$ mm) are negative. This implies that significant charging is occurring at temperatures warmer than -15°C . Thus the mixing increases the concentrations of both large and small ice below the heights below the -15°C level. The enhanced mixing also causes the model cloud to glaciate about 300 seconds sooner than the base case cloud since more ice is introduced at lower height earlier depleting the liquid water faster .

Table 5.5 shows a summary of the base and enhanced mixing runs. As indicated by the larger Q_{ntot} value, the enhanced mixing case has slightly more charging than

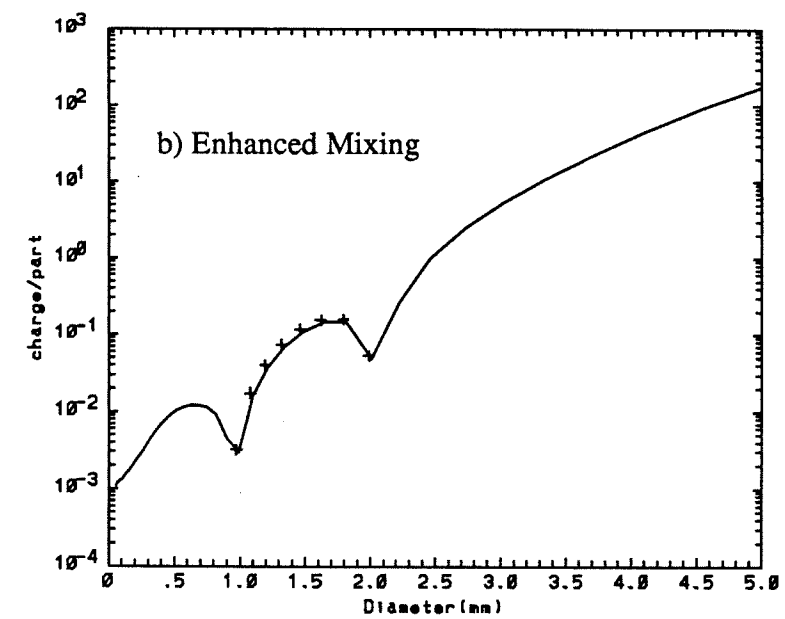
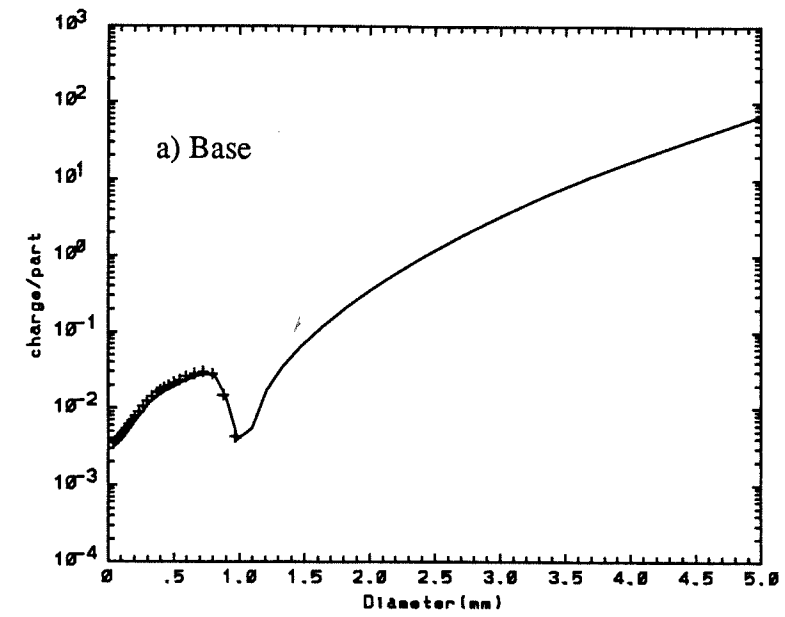


Figure 5.10: Mean charge per particle distributions for the (a) base case and (b) the enhanced mixing run at $t=3400$ seconds and $z=5.6$ km. The '+'s indicate positively charged particles.

the base case. The E_a in the enhanced mixing run is lower since the charge regions are more diffuse thus giving lower net charge densities. Also, the maximum field strength in the enhanced mixing run occurs approximately a minute later than in the base run. The primary difference in these runs is that the location of the main negative charge region is lower in the enhanced mixing case. Purely 1-dimensional models (Ziegler et al. 1986) have higher negative charge centers since updraft-downdraft mixing is neglected.

5.4 Stick efficiency - E_{si}

The ice-ice stick efficiency (E_{si} , section 2.3.3) was increased from 0.1 to 0.5 to determine its impact on the electrification. The increase in E_{si} decreases the number of separating ice-ice collisions about 44%. As a result, the maximum reflectivity in the increased E_{si} case is slightly larger. The reduction in the electric field and total negative charge values, by about 40 and 50% respectively, was due to the reduction of the number of collisions. Thus this parameter is important in the electrification process.

Table 5.6:

Stick efficiency Summary

Parameters	Maximum magnitudes for		
	dBZ_e	$Q_{ntot}(C)$	E (kV-cm ⁻¹)
$E_{si} = 0.1$	49.2	32.38	2.34
$E_{si} = 0.5$	49.6	15.60	1.45

5.5 Drop distribution

Table 5.7 shows the maximum values for the reflectivity, electric field, and total inner region negative charge for the runs in which the drop distribution was varied. The monodisperse distribution assumed that the all drops entering at the base of the model domain had the same size. The non-monodisperse distribution assumed the drop distribution specified by equation 3.5. Since these two drop distributions are different, the collection rates in the two runs would be different. However, as shown in Table 5.7, I found little variation between the cases primarily because the parameterization of the drop-ice interactions is simple (i.e. drop-ice collection efficiency = 1.0) and the warm cloud processes are generally unimportant here. Thus the effect of drop distributions is not important in the EM model electrification process.

Table 5.7:

Drop distribution electrification summary

Parameter	dBZ_e	$Q_{ntot}(C)$	E (kV-cm ⁻¹)
monodisperse	49.2	32.38	2.34
non-monodisperse	49.0	31.98	2.31

5.6 Critical charge transfer diameter - D_{crit}

The critical charge transfer diameter (D_{crit}) was used to represent the different surface types of the particles. Only particles $D \leq D_{crit}$ colliding with larger riming particles yielded charge separation. Table 5.8 shows a description and summary of the runs done to examine the electrification dependence on D_{crit} . All the summary values are very similar, indicating no strong dependence on D_{crit} . Figure 5.11 shows the magnitude of the charge density (ρ_c) and mean charge per particle (q_c) versus diameter at the main charging level ($Z=9.0$ km). Note the curves are identical for particle diameters up to 400μ and above 2.0 mm. The main differences in the q_c and ρ_c curves occur between the peaks in main charge carrying groups. Changes in D_{crit} do not affect the main charge carrying groups. If D_{crit} were below 400μ , it would begin to restrict collisions between the main groups of charge carriers, thus substantially reducing the charging. However, pushing D_{crit} deep into the small particle diameters goes against the primary assumption in using the D_{crit} parameter, i.e., that D_{crit} distinguished between particle with different surfaces. With $D_{crit} = 400\mu$, the size at which $q_c(D)$ switches sign is about 0.9 mm. This cross-over diameter occurs at the size where the amount of negative charge collected as a riming particle overcomes the positive charge collected as a small crystal. Raising D_{crit} to 800μ , shifts the sign cross-over diameter to about 1.2 mm since positive charging is permitted to larger diameter sizes (larger δq). Finally, at $D_{crit} = 1600\mu$, the cross-over diameter is 1.5 mm, less than D_{crit} itself. Because of the shape of the particle spectrum, particle with $D > 1.5$ mm do not have enough collisions with the

Table 5.8:

 D_{crit} run summary

run	D_{crit} (μ)	Maximum magnitude for		
		dBZ_e	Q_{ntot} (C)	E (kV-cm $^{-1}$)
a	400	49.1	28.94	2.24
b	800	49.2	32.38	2.34
c	1600	49.3	33.75	2.36

8/18/19

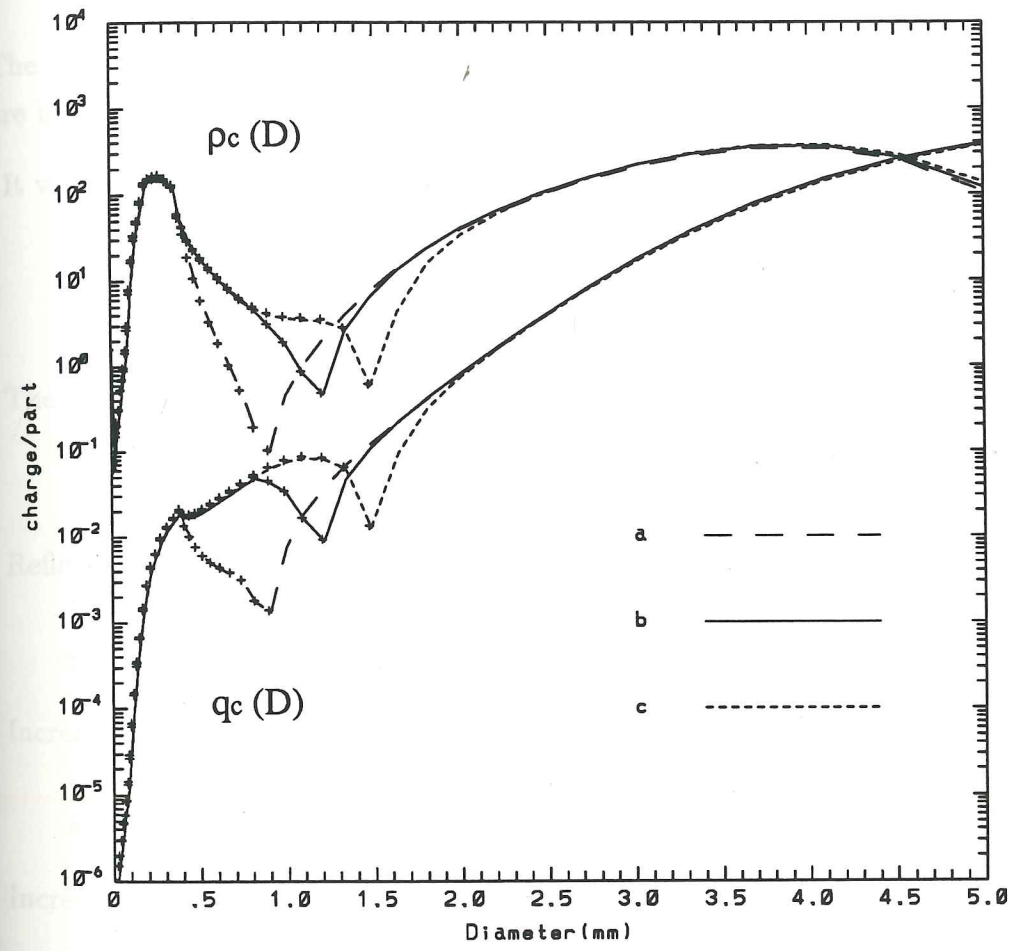


Figure 5.11: Magnitude of the charge per particle (q_c) and charge density (ρ_c) as function of diameter for the D_{crit} runs at $z=9.0$ km. The '+' indicate positive charge.

few bigger particles to overcome the charge gained through the collisions with many smaller particles. Thus the particle distribution itself determines the cross-over point so increasing D_{crit} above 1600μ would result in little change in electrification.

5.7 Summary

The sensitivity tests discussed above have indicated which parameters or processes are important to the electrification of the EM model clouds, and why.

It was shown that the particle and electrical development depends strongly on the choice of the ice crystal density via ρ_{crys} and riming diameter D_r . Combinations of these parameters which gave rapid particle growth to sizes greater than 200μ were able to produce strong electrification.

The electrification process was fairly insensitive to the choice for the ρ_a (rime density) parameterization. Although the lightest density form gave higher reflectivities, it produced Q_{tot} values lower than in the high density runs.

Reflectivity and E_a were relatively insensitive to the ice nucleus concentrations. However, increased ice concentrations increase overall charging and lower the main negative charge center.

Increasing the intra-cloud turbulent mixing substantially lowered the main negative charge center by laterally mixing higher concentrations of ice transported from higher altitudes in the outer region into the updraft.

Increasing the ice-ice stick efficiency lowers the Q_{tot} and E_a values proportionally.

The D_{crit} parameter and the initial drop distribution were not important parameters in either the microphysical or electrical evolution of the model cloud.

Chapter 6

Discussion

6.1 Assessment of the role of the ice-hail non-inductive charge separation mechanism in thunderstorm electrification.

One of the objectives of this study is to assess the importance of the ice-hail non-inductive charge separation mechanism in thunderstorm electrification. In Chapter 4, I compared the EM model results to parameters measured in-situ (charge density, particle distributions) and with remotely-sensed quantities (reflectivity, electric field). By and large, the primary parameter used in determining the importance for electrification of a specific charge mechanism is the magnitude of the electric field. Although the measurement of the electric field is subject to temporal and spatial variations, lightning is initiated at field strengths of 3-5 kV-cm⁻¹ (Latham, 1981). Thus the occurrence of a discharge provides a reasonable indication that electric fields of at least 3 kV-cm⁻¹ existed somewhere in the cloud. Therefore, one of the primary questions in assessing the importance of a charge mechanism is whether that charging mechanism can give rise to field strengths this magnitude to initiate lightning in a realistic amount of time.

In the EM mode runs, shown in Chapter 4, the time development of the electric field, given the initial cloud growth as the reference start time for the model, was in good agreement with observation (i.e. Figure 4.13); The predicted maximum electric field in the model occurred at about the same time as the observed discharge. There was enough charge separated, ± 30 to 40 C in the inner region alone, to support a single small discharge, even assuming a 30-50% efficiency of charge neutralization (Winn and Byerley, 1975). None of the model runs produced an electric field of 3 kV-cm⁻¹ or more, but many of the runs had electric fields within a factor of two of the breakdown field strengths. Since the typical electric field strength was of the same magnitude as required for lightning initiation, the ice-hail non-inductive charge separation mechanism studied here does seem a possible primary charging

mechanism in thunderstorms similar to the July 19, 1981 cloud.

Since the model only approximates the actual cloud, it is necessary to consider how the model results would be modified if the model were made more realistic. The most important constraint imposed by the model is its geometry. There are two main geometrical considerations: the symmetry and the horizontal coarse resolution. Since the model has axial symmetry, shear effects are not addressable. Although the actual cloud was weakly sheared, this shear was still enough to provide a directional preference for the falling precipitation, and hence downdrafts, from the upper regions of the cloud. This shearing would cause precipitation to fall out of the updraft. One possible consequence of this deficiency is that large particles in the model runs might stay in water rich inner region too long and hence undergo excessive charging. This would suggest the model is overestimating the charging and hence electric fields. However, because of the large particle in the updraft efficiency collecting water, this lack of shear may have been responsible for the early glaciation of the cloud (T). Thus with updraft unloading of precipitation, liquid water would persist longer, promoting a longer overall charging time. Also, precipitative falling from a sheared updraft may promote more efficient separation of the charge regions, giving rise to higher net charge densities.

The other main geometrical constraint is the coarse horizontal resolution. This area-averaged approach smears out many details which may lead to increased charging. For example, the updraft/downdraft interface which could be a major area of charging, as suggested by Dye et al. (1986), is crudely approximated by the inner/outer region interaction. The size and extent of such a region would be important to the charging process. Although the interface region would be smaller than the inner region of the EM model, concentrations of particles might be locally higher than the area-averaged concentrations in the model. The horizontal area averaging also smears out possible pockets of charge which could give localized areas of high fields.

Other non-geometrical considerations exist. Discharging effects, like screening layers and ion capture, may be important but have not been included.

This model study is an examination of the effectiveness of one particular charging mechanism. Because of the simple nature of the model, it cannot definitively determine whether this ice-hail non-inductive charge separation mechanism is operating alone in thunderstorms. However, this study does suggest that the ice-

hail non-inductive mechanism is likely to be important in the electrical evolution of certain classes of thunderstorms.

6.2 Thunderstorm electrification.

In a study of 20 New Mexico storms, Dye et al. (1989) concluded (1) that electrification is associated with vertical growth, (2) that electrification does not occur until after the radar tops exceed 8 km ($T < -20^{\circ}\text{C}$), and (3) that lightning is initiated when the radar tops have exceeded 9.5 km ($T < -30^{\circ}\text{C}$). From these observations, and the model results, a picture of TS electrification can be formed. Cloud top must reach temperatures below -20°C in order to have sufficient concentrations of small ice particles to initiate the electrification. Vertical motions are required to transport liquid water up to the colder temperatures to activate higher concentrations of ice. Mixing then moves ice to lower portions of the cloud for further charging. In clouds with cloud top temperatures warmer than -20°C , there are insufficient concentrations of small ice available to separate large amounts of charge.

To test this, I ran the EM model using only the $t=1500$ second velocity profile. Thus the cloud top height of this run never exceeded 7.6 km. The maximum value for the reflectivity was 50 dBZ_e while the maximum magnitude of the electric field was $1.09 \times 10^{-3} \text{ kV-cm}^{-1}$, three orders of magnitude less than the base run. There simply was not enough small ice for efficient charging in this simple model run. Since relatively few ice particles can yield the high reflectivities, reflectivity alone, as Dye et al. (1989) suggested, is not a good indicator of the electrical state of the cloud.

These results suggest that enough ice is formed at temperatures below -30°C to give rise to sufficient charging for lightning initiation. At these heights, charge will separate across the MPG interface (as described in section 4.2.1) which need not be a single surface. Also, turbulent transport will move ice particles to the lower portions of the cloud. The MPG interface would likely be the region of highest charging since only there would substantial concentrations of water, small and large ice coexist. This MPG interface idea is also consistent with observations (Lhermitte and Williams, 1985) that lightning initiation centers, and hence charging regions, are located on the upper fringes of reflectivity core.

Chapter 7

Conclusions and Final Remarks

7.1 Summary of this work

I have developed the kinematic (EM) model for examining the thunderstorm electrification process. Temperature and velocity fields were pre-determined from the T background model and used as input to the EM model. The model then calculated vapor, drop, ice, and charge concentrations as functions of time and height. Since this was a cold cloud base study, only deposition, collection, and primary glaciation were examined. Despite the model simplicity, our results have shown satisfactory agreement with the observed particle distributions, growth phase reflectivity profiles, and liquid water contents for the July 19, 1981 CCOPE cloud. The subsequent study of the ice-hail charge separation mechanism resulted in the following conclusions:

- The model calculated a maximum electric field of 2.3 kV-cm^{-1} , which occurred at the same time as the observed discharge. This result suggests that this charge transfer mechanism by itself might explain the primary electrical development in this storm. Also, the time development of the electric field was consistent with observations.
- Significant charges on particles developed several minutes before the strongest fields were observed which is consistent with observations.
- The positive-over-negative dipole structure was evident, in all runs, and the charge densities of each pole ($> 1 \text{ nC-m}^{-3}$) were consistent with observations.
- The electrification was strongly dependent on the ice crystal characteristics. Specifically, cases where the crystals grew to riming sizes ($> 400\mu$) fastest charge most efficiently. However, the characteristics of the large riming ice only had a minor influence on the charging. The electrification was not sensitive to

charge transfer critical diameter (D_{crit}) or the initial drop distribution. The electrification was sensitive to ice-ice sticking efficiency (E_{si}) as predicted.

- The location of the negative charge region was related to the interface between mixed phase and completely glaciated (MPG) parts of the cloud. The negative charge center was typically just below or at MPG cloud interface and the positive center was above the interface. The location of this MPG interface was determined by the cloud microphysics and dynamics. Model runs which had higher concentrations of ice at lower heights, via stronger eddy mixing or increased IN concentrations, had lower charge centers.

7.2 Suggestions for future work

Because of the complex nature of thunderstorms and the number of assumptions and simplification needed for modelling them, there is much room for improvements.

This thesis examined only one charge separation mechanism in one cloud case. Although these results indicate that this mechanism could explain the electrification process in this one cloud, other studies are required on different types of electrified clouds to further test this mechanism. Furthermore, as laboratory experiments improve and more information is obtained on this mechanism, further refinements to the charge parameterization can be made.

Several model simplifications can be improved. For example, the assumption that all ice particles are spheres is not truly realistic for the small ice particles. Other more realistic shapes could be used instead. Also, size dependent modifications to the ice-water and ice-ice stick efficiencies, for with the electrification is dependent, should be done. This model currently describes only cold microphysical processes. In order to examine other cloud cases, as suggested above, the microphysics must be expanded to include warm cloud processes such as drop coalescence and drop break-up. Expanding the microphysics to include snow would further aid in understanding the electrification. Also, the temperature and the microphysics should be calculated consistently to limit some of the thermodynamical/microphysical incompatibility problems encountered in this model version.

As radar measurements of thunderstorms become better and much more readily available, radar-derived wind fields will become more accessible. Since the EM

model is already in a kinematic framework and was originally designed to be easily incorporated into different geometries, creating a 2-dimensional version would be moderately easy. This would allow direct use of observed fields rather than those provided by another model. Thus intensive field programs, like CCOPE, are necessary for providing in-cloud and radar data by which modelers can use for comparison and model evaluation..

Finally, with an increased number of different cloud runs, a climatology of thunderstorms may be attempted. The goals would be to understand which environmental soundings are most likely to produce electrified storms and to predict the amount of lightning activity. In doing this, the parameters important in the electrification process can be further defined and understood.

LIST OF REFERENCES

- Asai, T., and A. Kasahara, A Theoretical Study of the Compensating Downward Motions Associated With Cumulus Clouds., *J. Atmos. Sci.*, **24**, 487-496, 1967.
- Auer, A. H., J. D. Marwitz, G. Vali, and D. L. Veal, Final Report to the National Science Foundation., Department of Atmospheric Resources, University of Wyoming, 94 pp, 1971.
- Baker, B., M. B. Baker, E. R. Jayaratne, J. Latham, and C. P. R. Saunders, The Influence of Diffusional Growth Rates on the Charge Transfer Accompanying Rebounding Collisions Between Ice Crystals and Hailstones., *Quart. J. R. Met. Soc.*, **113**, 1193-1215, 1987.
- Baker, M. B., and J. G. Dash, Charge Transfer in Thunderstorms and the Surface Melting of Ice., *J. Crys. Growth.*, **97**, 770-776, 1989.
- Battani, L.J., *Radar Observations of the Atmosphere.*, University of Chicago Press, Chicago, 1959.
- Beard, K.V. and H. T. Ochs, Charging Mechanisms in Clouds and Thunderstorms., in *The Earth's Electrical Environment*, p114-130, edited by P. Krider and R.G. Roble, National Academy Press, Washington D.C., 1986.
- Berry, E. X., Cloud Droplet Growth by Collection., *J. Atmos. Sci.*, **24**, 688-701, 1967.
- Berry, E. X., and M. R. Pranger, Equations for Calculating the Terminal Velocities of Water Drops., *J. Appl. Meteor.*, **13**, 108-113, 1974.
- Caranti, J.M., A.J. Illingworth, and S.J. Marsh, The Charging of Ice by Differences in Contact Potential., *J. Geophys. Res.*, **90**, 6041-6046, 1985.
- Cheng, C. P., Numerical Simulation of the Dynamics and Radar Echo Structure of Tropical and Mid-Latitude Convection., Ph.D Dissertation, University of Washington, 1981.

- Cotton, W.R., On Parameterization of Turbulent Transport in Cumulus Clouds, *J. Atmos. Sci.*, **32**, 548-564, 1975.
- Deshler, T., and G. Vali, The Accretion of Ice Particles by Rime During Dry Growth., *J. Atmos. Sci.*, **42**, 193-202, 1985.
- Dye, J. E., J. J. Jones, W. P. Winn, T. A. Cerni, B. Gardiner, D. Lamb, R. L. Pitter, J. Hallet, and C. P. R. Saunders, Early Electrification and Precipitation Development in a Small, Isolated Montana Cumulonimbus., *J. Geophys. Res.*, **91**, 1231-1247, 1986.
- Dye J.E., J.J. Jones, A.J. Weinheimer, and W.P. Winn, Observations Within Two Regions of Charge During Initial Thunderstorm Electrification., *Quart. J. R. Met. Soc.*, **114**, 1271-1290, 1989.
- Farley, R. D., Numerical Modeling of Hailstone and Hailstone Growth Part II; The Role of Low-density Riming Growth in Hail Production., *J. Appl. Meteor.*, **26**, 234-254, 1987.
- Farley, R. D. and H. D. Orville, Numerical Modeling of Hailstones and Hailstone Growth. Part 1 Preliminary Model Verification and Sensitivity Tests., *J. Climat. Appl. Meteor.*, **25**, 2014-2036, 1986.
- Fletcher, N.M., *The Physics of Rainclouds.*, Cambridge Univ. Press., 386 pp, 1962.
- Gardiner, B., D. Lamb, R. L. Pitter, J. Hallet, and C. P. R. Saunders, Measurements of Initial Potential Gradients and Particle Charges in a Montana Summer Thunderstorm., *J. Geophys. Res.*, **90**, 6079-6086, 1985.
- Gillespie, D. T., Three Models for the Coalescence Growth of Cloud Drops., *J. Atmos. Sci.*, **32**, 600-607, 1975.
- Hall, W. D., A Detailed Microphysical Model Within a Two Dimensional Dynamic Framework: Model Description and Preliminary Results., *J. Atmos. Sci.*, **37**, 2486-2507, 1980.
- Harris-Hobbs, R. L., and W. A. Cooper, Field Evidence Supporting Quantitative Predictions of Secondary Ice Production Rates., *J. Atmos. Sci.*, **44**, 1071-1082, 1987.

- Helsdon, J. H., and R. D. Farley, A Numerical Modeling Study of a Montana Thunderstorm: 1. Model Results Verses Observations Involving Nonelectrical Aspects., *J. Geophys. Res.*, **92**, 5645-5659, 1987a.
- Helsdon, J. H., and R. D. Farley, A Numerical Modeling Study of a Montana Thunderstorm: 2. Model Results Verses Observations Involving Electrical Aspects., *J. Geophys. Res.*, **92**, 5661-5675, 1987b.
- Heymsfield, A.J., The Characteristics of Graupel Particles in Northeastern Colorado Cumulus Congestus Clouds., *J. Atmos. Sci.*, **35**, 284-295, 1978.
- Heymsfield, A. J., C. A. Knight, and J. E. Dye, Ice Initiation in Unmixed Updraft Cores in Northeast Colorado Cumulus Congestus Clouds., *J. Atmos. Sci.*, **36**, 2216-2229, 1979.
- Heymsfield, A. J., and J. C. Pflaum, A Quantitative Assessment of the Accuracy of Techniques for Calculating Graupel Growth., *J. Atmos. Sci.*, **42**, 2264-2274, 1985.
- Hobbs, P. V., and A. L. Rangno, Ice Particle Concentrations in Clouds., *J. Atmos. Sci.*, **42**, 2523-2549, 1985.
- Illingworth, A.J., Charge Separation in Thunderstorms: Small Scale Processes., *J. Geophys. Res.*, **90**, 6026-6032, 1985.
- Illingworth, A.J., and J. Latham, Calculations of Electric Field Growth, Field Structure and Charge Distributions in Thunderstorms., *Quart. J. R. Met. Soc.*, **103**, 281-295, 1977.
- Illingworth, A.J., and J.M. Caranti, Ice Conductivity Restraints on the Inductive Theory of Thunderstorm Electrification., *J. Geophys. Res.*, **90**, 6033-6039, 1985.
- Jayaratne, E. R., C.P.R. Saunders, and J. Hallet, Laboratory Studies of the Charging of Soft-Hail During Ice Crystal Interactions., *Quart. J. R. Met. Soc.*, **109**, 609-630, 1983.
- Jayaratne, E. R., and C. P. R. Saunders, Thunderstorm Electrification: The Effect of Cloud Droplets., *J. Geophys. Res.*, **90**, 13063-13066, 1985.

- Jennings, S.G., Charge Separation due to Water Drop and Cloud Droplet Interactions in an Electric Field., *Quart. J. R. Met. Soc.*, **101**, 227-234, 1975.
- Jensen, J.B., P.H. Austin, M.B. Baker, and A.M. Blyth, Turbulent Mixing, Spectral Evolution and Dynamics in a Warm Cumulus Cloud., *J. Atmos. Sci.*, **42**, 173-192, 1985.
- Keith, W. D., and C. P. R. Saunders, Charge Transfer During Multiple Large Ice-Crystal Interactions with a Riming Target., *J. Geophys. Res.*, **94**, 13,103-13,106, 1989.
- Kessler, E. III, On the Distribution and Continuity of Water Substance in Atmospheric Circulation., *Meteor. Monog.*, **3**, 32 pp. AMS, 1969.
- Knight, C.A., Lagrangian Modeling of the Ice Process: A First Echo Case, *J. Atmos. Sci.*, , in press, 1990.
- Krehbiel P.R., The Electrical Structure of Thunderstorms., in in *The Earth's Electrical Environment*, p90-113, edited by P. Krider and R.G. Roble, National Academy Press, Washington D.C, 1986.
- Kuettner J.P., Z. Levin, and J.D. Sartor, Thunderstorm Electrification - Inductive or Non-Inductive?, *J. Atmos. Sci.*, **38**, 2470-2484, 1981.
- Latham J., The Electrification of Thunderstorms., *Quart. J. R. Met. Soc.*, **107**, 277-298, 1981.
- Latham, J., and J.E. Dye, The Electrical Development of a Small Thunderstorm., *J. Geophys. Res.*, **94**, 13,141-13,144, 1989.
- Lhermitte R., and E.R. Williams, Thunderstorm Electrification: A Case Study., *J. Geophys. Res.*, **90**, 6071-6078, 1985.
- Macklin, W.C., The Density and Structure of Ice Formed by Accretion, *Quart. J. R. Met. Soc.*, **88**, 30-55, 1962.
- Martin, P.F., and W.C.A. Hutchinson, Melting Electrification of Single Particles in Simulated Free Fall, in *Electrical Processes in Atmospheres*, p.302-308, edited by H. Dolezalek and R.Reiter, Steinkopff, Darmstadt, 1977.

- Mason, B.J., The Generation of Electric Charges and Fields in Thunderstorms, *Proc. R. Soc.*, **A415**, 303-315, 1988.
- Moore, C.B., Charge Generation in Thunderstorms., in *Problems in Atmospheric Electricity*, edited by C.S. Coronti, pp. 255-262, Elsevier, N.Y, 1965.
- Moore, C.B., B. Vonnegut, B.A. Stein, and H.J. Survilas, Observations of Electrification and Lightning in Warm Clouds., *J. Geophys. Res.*, **65**, 1907-1910, 1960.
- Mossop S.C., The Influence of Drops Size Distribution on the Production of Secondary Ice Particles During Graupel Growth., *Quart. J. R. Met. Soc.*, **104**, 323-330, 1978.
- Paluch I.R., The Entrainment Mechanism in Colorado Cumuli., *J. Atmos. Sci.*, **36**, 2467-2478, 1979.
- Pflaum, J.C., and H.R. Pruppacher, A Wind Tunnel Investigation of the Growth of Graupel Initiated From Frozen Drops, *J. Atmos. Sci.*, **36**, 680-689, 1979.
- Pruppacher, H.R., and J.D. Klett, *Microphysics of Clouds.*, D.Reidel. Hingham, Massachusetts, 1978 .
- Rawlins F., A Numerical Study of Thunderstorm Electrification using a Three Dimensional Model Incorporating the Ice Phase., *Quart. J. R. Met. Soc.*, **108**, 779-800, 1982.
- Reynolds, S.E., M. Brook, and M.F. Gourley, Thunderstorm Charge Separation., *J. Meteorol.*, **14**, 426-436, 1957.
- Sartor, J.D., Inductive Charging of Clouds., *J. Atmos. Sci.*, **38**, 218-220, 1981.
- Shewchuk, S.R., and J.V. Iribarne, Charge Generation During Splashing of Large Drops on Ice., *Quart. J. R. Met. Soc.*, **97**, 272-282, 1971.
- Smagorinsky, J., General Circulation Experiments with the Primitive Equations, 1, The Basic Experiments., *Mon. Wea. Rev.*, **14**, 1156-1175, 1963.
- Smolarkiewicz, P. K., A Simple Positive Definite Advection Scheme with Small Implicit Diffusion., *Mon. Wea. Rev.*, **111**, 479-486, 1983.

- Smolarkiewicz, P. K., A Fully Multidimensional Positive Definite Advective Transport Algorithm with Small Implicit Diffusion., *J. Comp. Phys.*, **54**, 325-362, 1984.
- Stephens, M.A., A Simple Ice Phase Parameterization., *Atmospheric Science Paper no. 319*, Dept of Atmos.Sci. Colorado State University, 122 pp, 1979.
- Takahashi, T., Riming Electrification as a Charge Generation Mechanism in Thunderstorms., *J. Atmos. Sci.*, **35**, 1536-1548, 1978.
- Takahashi, T., A Numerical Simulation of Winter Cumulus Electrification. Part 1: Shallow Cloud., *J. Atmos. Sci.*, **40**, 1257-1280, 1983.
- Takahashi, T., Thunderstorm Electrification - A Numerical Study., *J. Atmos. Sci.*, **41**, 2541-2558, 1984.
- Taylor, G.R., A Numerical Investigation of Sulfate Production and Deposition in Midlatitude Continental Cumulus Clouds., Ph.D Dissertation, University of Washington, 1987.
- Taylor, G.R., Sulfate Production and Deposition in Midlatitude Continental Cumulus Clouds, Part I: Cloud Model Formulation and Base Run Analysis., *J. Atmos. Sci.*, **46**, 1971-1990, 1989.
- Tzur, I., and Z. Levin, Ions and Precipitation Charging in Warm and Cold Clouds as Simulated in One-Dimensional Time-Dependent Models., *J. Atmos. Sci.*, **38**, 2444-2461, 1981.
- Vali, G., T. Deshler, and D.C. Rodgers, Concentrations of Ice Nuclei of Different Modes of Activation., Preprints, *Eleventh International Conf. on Atmospheric Aerosols, Condensation, and Ice Nuclii*, V. II., Hungarian Meteorol. Soc., 105-109, 1984.
- Vonnegut, B., Possible Mechanism for the Formation of Thunderstorm Electricity., *Bull. Am. Meteor. Soc.*, **34**, 378-381, 1953.
- Williams, E.R., The Tripole Structure of Thunderstorms., *J. Geophys. Res.*, **94**, 13,151-13,167, 1989.

- Williams, E.R., C.M. Cooke, and K.A. Wright, Electrical Discharge Propagation in and Around Space Charge Clouds., *J. Geophys. Res.*, **90**, 6059-6070, 1985.
- Winn, W.P., and L.G. Byerley III, Electric Field Growth in Thunderstorms., *Quart. J. R. Met. Soc.*, **101**, 979-993, 1975.
- Workman, E.J., and S.E. Reynolds, A Suggested Mechanism for the Generation of Thunderstorm Electricity., *Phys. Rev. Lett.*, **74**, 709, 1948.
- Yau, M., A Two-cylinder Model of Cumulus Cells and its Application in Computing Cumulus Transports., *J. Atmos. Sci.*, **37**, 2470-2485, 1980.
- Young, K.C., A Numerical Simulation of Wintertime, Orographic Precipitation: Part 1. Description of Model Microphysics and Numerical Techniques., *J. Atmos. Sci.*, **31**, 1735-1748, 1974.
- Ziegler, C. L., P. S. Ray, and D. R. MacGorman, Relations of Kinematics, Microphysics and Electrification in an Isolated Mountain Thunderstorm., *J. Atmos. Sci.*, **43**, 2098-2114, 1986.

Appendix A

Derivation of Advective Equations.

The EM3 model uses generalized area-averaged equations which are similar to those used by T, Asai and Kasahara (1967), and Yau (1980). The basic anelastic continuity equation for a generalized density (ρ) in cylindrical coordinates is:

$$\frac{\partial \rho}{\partial t} + \frac{1}{r} \frac{\partial}{\partial r}(r \rho u) + \frac{\partial}{\partial z}(\rho w) = S, \quad (\text{A.1})$$

where S is the sink/source term. Mass continuity is found from equation A.1 by setting the source and time-dependent terms to zero and ρ equal to the base state density (ρ_o). Thus mass continuity is given by:

$$\frac{1}{r} \frac{\partial}{\partial r}(r \rho_o u) + \frac{\partial}{\partial z}(\rho_o w) = 0. \quad (\text{A.2})$$

The above equations are then area-averaged by integrating:

$$\overline{(\quad)}_{i,o} \equiv \frac{1}{\mathcal{A}_{i,o}} \int_0^{2\pi} \int_{0,a}^{a,b} (\quad) r dr d\theta \quad (\text{A.3})$$

where \mathcal{A} is the cross-sectional area of the inner or outer region. The subscripts a and b are for the inner-outer boundary and the outer-environmental boundary, respectively. Doing this gives the basic area-averaged advective equations for a generalized density (ρ) in the inner region and outer region (with over-bars dropped) as:

$$\frac{\partial \rho_i}{\partial t} = -\frac{\partial(\omega_i \rho_i)}{\partial z} - \rho_a \frac{\partial w_i}{\partial z} - \frac{2}{a}(\rho_i' u')_a - \frac{\partial}{\partial z}(\omega_i' \rho_i') + S_{e_i} \quad (\text{A.4})$$

$$\begin{aligned} \frac{\partial \rho_o}{\partial t} = & -\frac{\partial(\omega_o \rho_o)}{\partial z} + \left[\rho_b \frac{\partial w_o}{\partial z} + (\rho_b - \rho_a) \frac{a^2}{(b^2 - a^2)} \frac{\partial w_i}{\partial z} \right] + \\ & \frac{2a}{(b^2 - a^2)}(\rho_i' u')_a - \frac{\partial}{\partial z}(\omega_o' \rho_o') + S_{e_o} \end{aligned} \quad (\text{A.5})$$

where ω is the vertical air velocity for the vapor or the difference between the air and fall velocity for particles. The densities at the inner-outer boundary and outer-environment boundary are designated by ρ_a and ρ_b , respectively. Deviations from

the mean are designated by primes. The terms on the rhs of equations A.4 and A.5 are the vertical advection, dynamic entrainment, lateral eddy flux, vertical eddy flux, and a generalized source/sink term. The outer region/environment lateral eddy flux term, which is not shown, has been set to zero in the model for simplification.

To close the above equations, the eddy flux terms and the dynamic entrainment parameters (ρ_a , ρ_b) must be specified. Following T, the value of ρ_a is either ρ_i or ρ_o , as determined by the direction of the horizontal bulk flow (u_a) between the inner and outer regions:

$$\rho_a = \begin{cases} \rho_i, & u_a \geq 0 \\ \rho_o, & u_a < 0. \end{cases} \quad (\text{A.6})$$

For ρ_b , I used the flux-weighted form of Cotton (1975) based on the assumption that air near the boundary is a mixture of cloudy and environmental air. Thus,

$$\rho_b = \begin{cases} \frac{F_{lat}\rho_o + F_{up}\rho_{ou}}{F_{lat} + F_{up}}, & u_b \geq 0 \\ \frac{F_{lat}\rho_{env} + F_{up}\rho_{ou}}{F_{lat} + F_{up}}, & u_b < 0 \end{cases} \quad (\text{A.7})$$

where F_{lat} ($= 2\pi b u_b dz$) is the lateral flux, F_{up} ($= \pi(b^2 - a^2)w_o$) is the vertical upstream flux, ρ_{ou} is the upstream density, and ρ_{env} is the environmental density.

Following T, the eddy mixing terms are calculated using a Smagorinsky (1963) form of the eddy diffusivity and are given by

$$(\omega_i' \rho_i') = -K_a(r=0) \frac{\partial \rho}{\partial z} \quad (\text{A.8})$$

$$(\rho_i' u')_a = -K_a(r=a) \frac{\partial \rho}{\partial r} \quad (\text{A.9})$$

$$(\omega_o' \rho_o') = -K_a(r=0.5(a+b)) \frac{\partial \rho}{\partial z} \quad (\text{A.10})$$

where

$$K_a(r=x) = \alpha_m \sigma_i \frac{(k_1 \Lambda)^2}{\sqrt{2}} |D_{ij}|_{r=x} \quad (\text{A.11})$$

and α_m is a mixing constant ($=1$ or $1/3$) used to examine the effects of mixing in the model, σ_i is the Prandtl number ($=3.0$), Λ is the averaging length, k_1 is a constant set to 0.28, and $|D_{ij}|$ is the magnitude of the deformation tensor of an anelastic medium and is evaluated at $r=0$, a , and $0.5(a+b)$ depending on the mixing term used. These terms are identical to those used by T except that the buoyancy modification to λ was not done.

Appendix B

Crystal density determination.

The initial values for ρ_{crys} was determined from two means. First, ρ_{crys} was estimated by determining the density needed to give a sphere the same radius as a plate assuming that the plate and sphere had the same mass. Thus the dimensions of the plate and sphere are related by

$$\frac{4}{3}\pi R^3 \rho_{sphere} = M = \pi R^2 h \rho_{plate} \quad (B.1)$$

where R is the radius of the plate and sphere, h is the width of the plate, and ρ_{sphere} and ρ_{plate} are the densities of the sphere and plates respectively. From the above equation, the ratio of the sphere and plate densities is

$$\frac{\rho_{sphere}}{\rho_{plate}} = \frac{3h}{4R} \quad (B.2)$$

Heymsfield (1972) found that h was related to R by

$$h = 0.449 (2R)^{0.449} \text{ (mm)} \quad (B.3)$$

for $R \leq 0.2$ mm. Substituting this equation into equation B.2, we get

$$\frac{\rho_{sphere}}{\rho_{plate}} = 0.046 R^{-.551} \text{ (R in mm)} \quad (B.4)$$

Heymsfield found the densities for pure plates is 0.9 g-cm^{-3} . However, Heymsfield also found plates with air in them which had a lower density of 0.6 g-cm^{-3} . Table B.1 show the results of equation B.4 for these two plate densities at different radius values. The values range from 0.36 to 0.07 depending on the size and assumed ρ_{plate} value.

Table B.1:

Calculated $\frac{\rho_{sphere}}{\rho_{plate}}$ and densities assuming sphere with same radius as an equal mass plate.

R in mm	$\frac{\rho_{sphere}}{\rho_{plate}}$	ρ_{sphere}	
		$\rho_{plate} = 0.9$	$\rho_{plate} = 0.6$
0.02	0.4	0.36	0.24
0.04	0.27	0.24	0.16
0.08	0.18	0.16	0.11
0.10	0.16	0.14	0.01
0.20	0.11	0.10	0.07

Secondly, T provides mass and diameter relations as given in equation B.5.

$$D_c = \alpha(M_s)^\beta = \begin{cases} 16.286(M_s)^{0.5} & M_s < 10^{-10} \\ 6.072(M_s)^{0.5} & 10^{-10} < M_s < 10^{-8} \\ 1.585(M_s)^{0.417} & M_s > 10^{-8} \end{cases} \quad (B.5)$$

where units are in MKS. By assuming a spherical shape, a density can be found by

$$\rho_{crys} = \frac{6 M_s}{\pi D_c^3} = \frac{1.91}{\alpha^3} (M_s)^{1-3\beta} \quad (B.6)$$

With $M_c < 10^{-10}$ and $M_c > 10^{-8} kg$, the snow density is less than 0.1 g-cm^{-3} . Between $10^{-10} < M_c < 10^{-8}$ the density ranges from 0.85 to 0.08 g-cm^{-3} . For example, at $D_c = 200$ and 400μ , $\rho_s = 0.2$ and 0.12 g-cm^{-3} respectively. Inspection of the T snow contents showed M_c was typically greater than 10^{-8} kg so the snow density was typically below 0.1 g-cm^{-3} .

Since the first argument suggest an ice density near 0.2 g-cm^{-3} and the T argument below 0.1 g-cm^{-3} , I selected an initial ice density values of 0.1 g-cm^{-3} .

Appendix C

Derivation of Z to Z_e ice correction

From equation 4.2 which relates the radar reflectivity to the power returned, the reflectivity assuming an ice distribution (Z_i) can be easily related to Z_e by

$$Z_i |K_i|^2 = \frac{\overline{P_r} r^2}{C} = Z_e |K_w|^2 \quad (\text{C.1})$$

where $|K_i|^2$ and $|K_w|^2$ are the complex index of refraction factors for ice and water respectively. Since the particle distribution in the electrification model is readily accessible, it is much more convenient to convert the model Z to Z_e . Rewriting equation C.1 to solve for Z_e , we find

$$Z_e = \frac{|K_i|^2}{|K_w|^2} Z_i \quad (\text{C.2})$$

It has been shown (Mason, 1957) that

$$|K_i|^2 = \left(\frac{\rho}{\rho_w} \right)^2 |K_*|^2 \quad (\text{C.3})$$

where ρ and ρ_w are the densities of the ice and water, and $|K_*|^2$ is the complex index of refraction factor of hypothetical ice with ρ_w . By using the equations for $|K_i|^2$ (C.3), Z_e from Z_i (C.2), and Z from the model distribution (4.1), the final equation for Z_e of the model is

$$Z_e(\text{mod}) = \frac{|K_*|^2}{|K_w|^2 (\rho_w)^2} \sum_k \rho_k^2 n(k) D_k^6 \quad (\text{C.4})$$

VITA

Kent Weston Norville was born in Pasadena, CA, on December 9, 1959. After graduating from Glendora High School in 1978, he spent a year and a half at Azusa Pacific College before transferring to California Polytechnic State University at San Luis Obispo where he received a B.S. degree with honors in Physics in 1983. He then spent a month in New Zealand collecting igneous rock and sediment samples for Professor Kenneth Hoffman's paleomagnetic research. After that trip, he spent six months working as a Coop engineer in San Jose, CA. In the Fall of 1983, he began graduate studies in Geophysics at the University of Washington working with Professor Robert Holzworth on the Electrodynamics of the Middle Atmosphere (EMA) superpressure balloon project. Through this work, he became interested in trying to understand the electrical behavior of the lower atmosphere with particular emphasis on the electric global circuit (of which it is thought that thunderstorms are the source). As a result of this work, the following papers were published:

Global Circuit Variability From Multiple Stratospheric Electrical Measurements, by K.W. Norville and R.H. Holzworth, *J.Geophys.Res.*, 92, 5685-5695, 1987.

Solar Flare Perturbations in Stratospheric Current Systems, by R.H. Holzworth, K.W. Norville, and P.R. Williamson, *Geophys.Res.Lett.*, 14, 852-855, 1987.

Stratospheric Conductivity Variations Over Thunderstorms, by R.H. Holzworth, K.W. Norville, P.M. Kintner, and S. Powell, *J.Geophys.Res.*, 91, 13,257, 1986.

In the last three years he looked at the source of the global circuit: thunderstorms. That is what this dissertation is all about.

1719 78